

Microfluidic Flow in the Insect Respiratory System

Joel F. Garrett

Dissertation submitted to the faculty of
Virginia Tech
in partial fulfillment of the requirements for the degree of

Doctor of Philosophy
in
Biomedical Engineering

John J. Socha, Chair
Rafael Davalos, Co-chair
Jon Harrison
Anne Staples
Mark Stremler

September 25, 2020
Blacksburg, Virginia

Keywords: Fluid Dynamics, Entomology, Microfluidics, Hissing Cockroach, Simulation

Copyright © 2020 Joel Garrett

Academic Abstract

Microfluidic Flow in the Insect Respiratory System

Joel Garrett

In this dissertation, we examine how advective and diffusive flows are created in the insect respiratory system, using a combination of direct biological studies and computational fluid dynamics simulations. The insect respiratory system differs significantly from the vertebrate respiratory system. While mammals use oxygen-carrying molecules such as hemoglobin, insects do not, favoring the direct delivery of oxygen to the tissues. An insect must balance advective flow with diffusive flux in order to sustain the appropriate oxygen concentrations at the tissue level. To better understand flow creation mechanisms, we studied the Madagascar hissing cockroach. In Chapter One, we used x-ray imaging to identify how tracheal tube compression, spiracular valving, and abdominal pumping coordinate to produce unidirectional flow during active respiration. In Chapter Two, we altered the environmental conditions by exposing the animals to various levels of hypoxia and hyperoxia, then examined how they changed their respiratory behaviors. In Chapter Three, we used our previous findings to construct a simulated insect respiratory system to parametrically study the effects of network geometry and valve timing on the creation of unidirectional advective flow and diffusive flux. These results can be used to inform future studies of the insect respiratory system, as well as act as the basis for bio-inspired microfluidic devices.

General Audience Abstract

Microfluidic Flow in the Insect Respiratory System

Joel Garrett

The insect respiratory system works through the direct delivery of oxygen to the tissues. This occurs via a complex network of pumps, tubes, valves, and other structures that facilitate flow. These mechanisms allow insects to survive and prosper under a wide range of environmental and physiological conditions. While these structures have been studied extensively in a wide range of insect species, there are still many aspects of the respiratory system that remain unexplored. Here, we use the Madagascar hissing cockroach to examine how both bulk flow and diffusion are created in some types of insect respiratory systems. First, in Chapter One, we studied the animal under normal environmental conditions in order to determine how abdominal pumping, tracheal tube collapse, and spiracular valving are coordinated. Then, in Chapter Two, we exposed the animals to a range of oxygen concentrations to identify how the animals respond to varying environmental conditions. Finally, in Chapter Three, we constructed a simulated insect respiratory system to parametrically study the effects of network geometry and valve timing on the creation of advective and diffusive flow. By combining these three studies, we were able to improve our understanding of flow creation in the insect respiratory system.

Dedication

For my parents, Randy and René Garrett, for putting up with all my nonsense.

Acknowledgements

I would like to acknowledge the many people who have made this dissertation work possible. First and foremost, I'd like to thank my advisors, Jake Socha and Rafael Davalos, who pushed me to be a better scientist and engineer. I'd also like to thank my lab mates Khaled Adjerid, Hodjat Pendar, and Melissa Kenny who supported me throughout this work. I'd like to thank my committee members Mark Stremmer, Jon Harrison, and Anne Staples for their insight and input toward the development of this project.

This research was supported by NSF grants #0938047, #0966125, #1558052 and the Virginia Tech BIOTRANS program.

Contents

Academic Abstract.....	ii
General Audience Abstract.....	iii
Dedication.....	iv
Acknowledgements.....	v
Contents.....	vi
Chapter 1: The mechanical components of respiration	1
Introduction	1
Methods.....	3
Animals.....	4
Video collection: Setup 1	4
Video collection: Setup 2	6
Analysis of tracheal compression and internal spiracle state	7
Analysis of abdominal pumping	9
Results.....	11
Discussion	13
Abdominal pumping and tracheal tube collapse.....	13
Coordination between abdominal pumping and spiracular valving.....	13
Internal spiracle dynamics	13
Conclusion.....	14
Chapter 2: The insect's response to hypoxia and hyperoxia	14
Introduction	14
Methods.....	15
Experimental Setup	16
Oxygen Control.....	17
Video Digitization	17
Results.....	19
Discussion	22
Chapter 3: A computational fluid dynamics simulation of the insect respiratory system	25
Introduction	25
Previous work.....	25
Methods.....	26
Results.....	28

Discussion	32
Conclusion.....	35
Hissing cockroach respiratory coordination	35
The response to hypoxia and hyperoxia	35
Simulating the insect respiratory system	36
Future work.....	36
References	37
Appendix A – Plots of abdominal movement	41
Appendix B – Plots of spiracle state	47

Chapter 1: The mechanical components of respiration

Introduction

To begin this study, we examined how the various components of the Madagascar hissing cockroach (*Gromphadorhina portentosa*) respiratory system interact to produce a net unidirectional flow in from the thorax and out through the abdomen. The components we investigated were the collapsible tracheal network, the abdominal pump, and the spiracular valves. We studied the animals using conventional video and phase-contrast x-ray. In the Madagascar hissing cockroach, abdominal compression seems to actuate tracheal tube collapse, which produces a pressure gradient that drives flow through the tube system. By working in concert with spiracular valves in the thorax and abdomen, a net unidirectional flow of air is created (Heinrich et al., 2013).

Flow systems that incorporate pumping and valving depend on the temporal specifics of its components to operate efficiently (Groenewald et al., 2012). In humans, even minute abnormalities in respiratory coordination can potentially lead to reduced functionality, damage to the circulatory system, and a shortened lifespan (Ambler et al., 2005; Gelson et al., 2007). Sleep apnea can arise from compounding irregularities in ventilatory control (Hudgel et al., 1998; Wellman et al., 2004) and results in billions of dollars of additional medical costs annually (Hillman et al., 2006). Respiratory patterns involving the diaphragm, upper airway musculature (such as the glossal and nasal valves), mouth, and lungs have been examined thoroughly by exercise physiologists (Askanazi et al., 1979; Mathew & Farber, 1983).

Many studies have confirmed that maintaining proper ventilatory timings are essential for maximizing athletic performance in humans (Caretti et al., 1992; Lucía et al., 1999), horses, and dogs (Daley et al., 2013). The importance of valve timing in automotive (Lancefield et al., 2000; Nouhov, 2004; Stein et al., 2014) engineering is likewise well-studied.

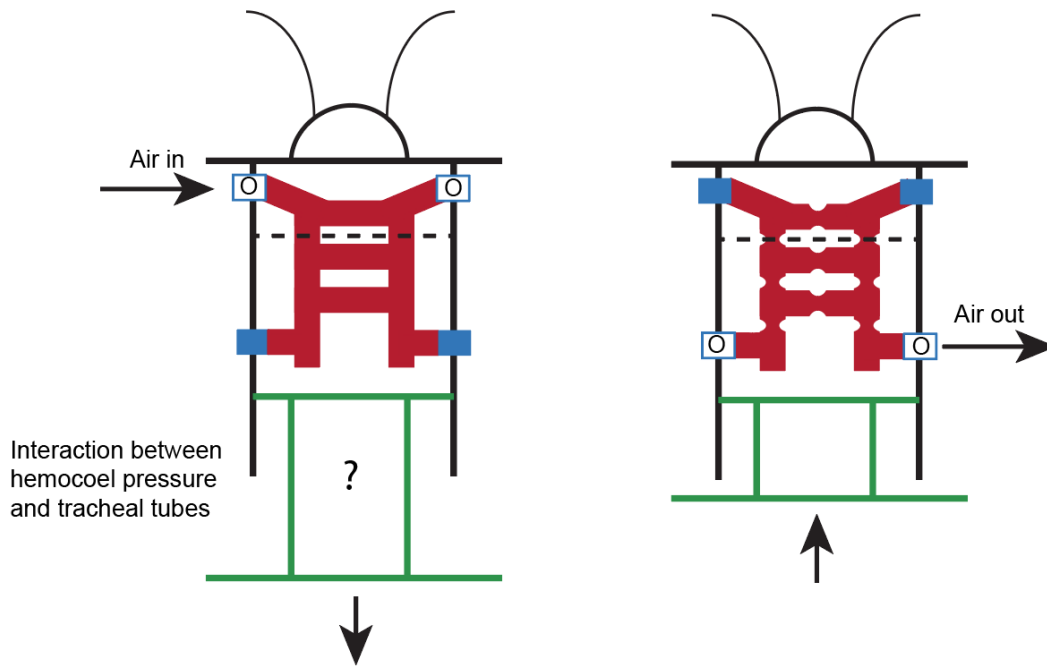


Figure 1: A proposed mechanism for hissing cockroach respiration. These diagrams demonstrate how abdominal compression (right, green) may relate to tracheal tube (red) collapse at pre-determined points and spiracular valving (blue) to produce a net unidirectional airflow in (left) from the thoracic spiracles and out (right) through the abdominal spiracles. The precise mechanisms by which abdominal compression results in tracheal tube collapse are still unknown.

Respiratory function should be dependent on the pump, tubes, and valves working with a tight, controlled coordination (Sherman, 1981). Although some details can be derived from physical principles – a tube collapses, one valve opens, another valve closes, and flow is created - specific details of the temporal coordination of the insect respiratory system are substantially less understood.

The external pumping and spiracular valving behaviors of the Madagascar hissing cockroach have been linked with the production of unidirectional airflow (Heinrich et al., 2013), and the animal's large size and calm demeanor makes the species a good candidate for our study to offer a quantitative characterization of the movement patterns and temporal coordination of abdominal compression, tracheal tube collapse, and spiracular valving during active respiration to yield enhanced temporal and spatial clarity of its respiratory patterns

This system contains components that operate internally (the tracheal network), externally (the abdominal pump), and at the interface (the spiracles). It is essential to consider both internal and external mechanisms to fully understand the biological and fluid dynamics of the insect respiratory system. The tracheal network and spiracular valves are very small (on the order of tens to hundreds of microns) and movements often occur at the sub-second level, so high spatial and temporal resolutions are important for classifying these behaviors. Additionally, the material properties of tracheal tube

tissue suggest a nonlinear response to pressure actuation (Webster et al., 2011) so abdominal movement alone cannot be used to characterize the internal dynamics of the system.

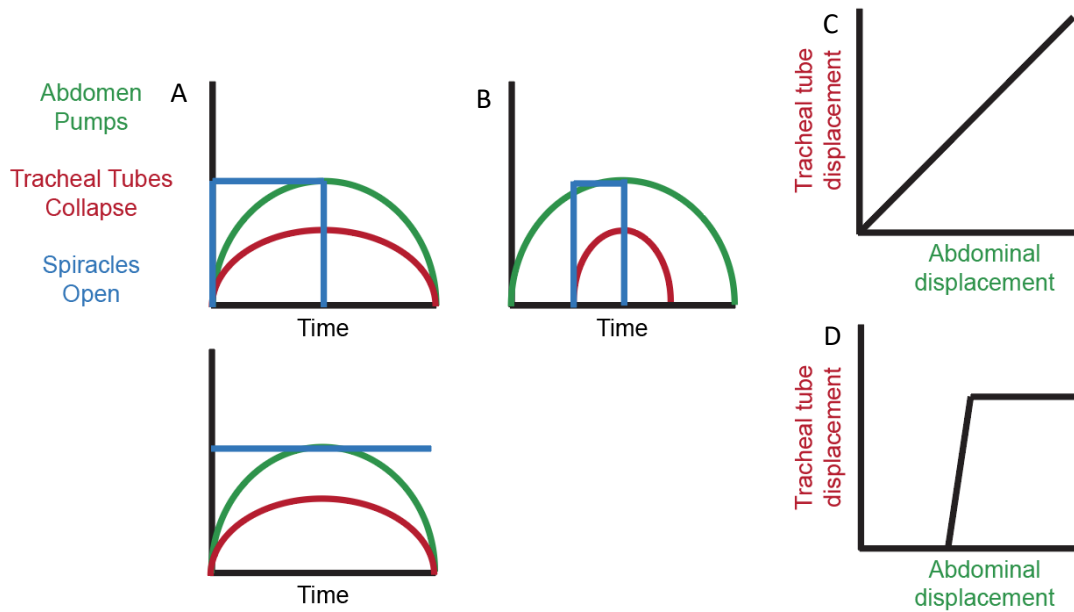


Figure 2: Different modalities of spiracle behavior according to abdominal pumping and tracheal tube collapse behavior. In A & C we see what should happen if tracheal collapse happens immediately in concert with abdominal compression, assuming a linear tracheal tube collapse. In B & D we instead observe what should happen if tracheal collapse is non-linear.

Therefore, we used a combination of both external video and internal x-ray footage to assess the movement and timing of these respiratory structures. We know that the behaviors of the abdomen and spiracle produce a net unidirectional flow (Heinrich et al., 2013), and that there is a neurological linkage between abdominal compression and spiracular opening (Nelson, 1979). However, we still lack a fine understanding of how tracheal collapse coincides with abdominal compression, as well as a mechanistic understanding of spiracular valving and how its timing relates to tracheal collapse.

We hypothesize that, under normal and active breathing conditions (i.e. not during discontinuous gas exchange), the animal will coordinate its abdominal pumping with spiracular valving in a way consistent with the observed nonlinear collapse of tracheal tubes and minimize the amount of time that spiracles are left open. Understanding this facet of respiratory coordination in the Madagascar hissing cockroach will open new avenues of study for other insect species.

Methods

We examined the respiratory structures of living Madagascar hissing cockroaches, combining internal X-ray video with external footage to analyze the timing and kinematics of the abdominal pump, tracheal tube collapse, and spiracular movement in actively respiring animals.

Animals

We chose the Madagascar hissing cockroach (*Gromphadorhina portentosa*) for study because of its large size (~5 cm body length, ~5 – 9 g mass) and its large, visible spiracle anatomy. These traits allowed us to precisely assess the movement of respiratory structures using video. Twenty adult roaches (15 male and 5 female) were examined in total. The roaches originated from our colony at Virginia Tech, where they were given water and food (bran and dry dog food) *ad libitum*, kept at approximately 27 °C with a lightless heating coil and under-tank heating pad, and subjected to natural light cycles. In our roach cohort, females were significantly larger than males ($m = 8.45 \pm 1.01$ g for females, $m = 6.57 \pm 0.86$ g for males, Student's t-test, $p < 0.05$).

All experiments were conducted at beamline 32-ID at the Advanced Photon Source (APS) in three experimental sessions (August 2013, July 2014, and November 2014). Roaches were transported by car to the Advanced Photon Source at Argonne National Laboratory and housed in a similar habitat to the Virginia Tech lab. To prepare for the trials, each animal was anesthetized by exposure to nitrogen gas. Prior to the trials, we measured body length with a ruler and mass with a balance (TS400D, Ohaus Corporation, Parsippany, NJ), and then mounted the animal to a frame (Figure 1B,C). Across experimental sessions, the overall design of the trials was consistent, but the setup was modified for small improvements between sessions, described below.

Video collection: Setup 1

Nine male roaches were examined during the August 2013 session. In this experimental setup, animals were mounted to a frame composed of a small sheet of polyimide film (Kapton, E. I. du Pont de Nemours and Company, Wilmington, DE) suspended in a 100 mm x 100 mm aluminum brace (Figure 1b). Kapton tape was used to secure the legs individually. The head and thorax were covered with opaque black tape (Pro-Gaff by ProTapes, North Brunswick, NJ) to further secure the animal. The animal was illuminated using two LED arrays (Litepanels MicroPro, Vitec Videocom, Inc, London, UK).

Synchrotron X-ray video was collected following the procedures outlined by Socha *et al* (Socha & De Carlo, 2008). This footage was recorded to tape with a beam energy of 30 keV, a beam gap of 22 mm, and a taper of 5.0 mm, at a resolution of 720 x 480 pixels at 30 frames per second.

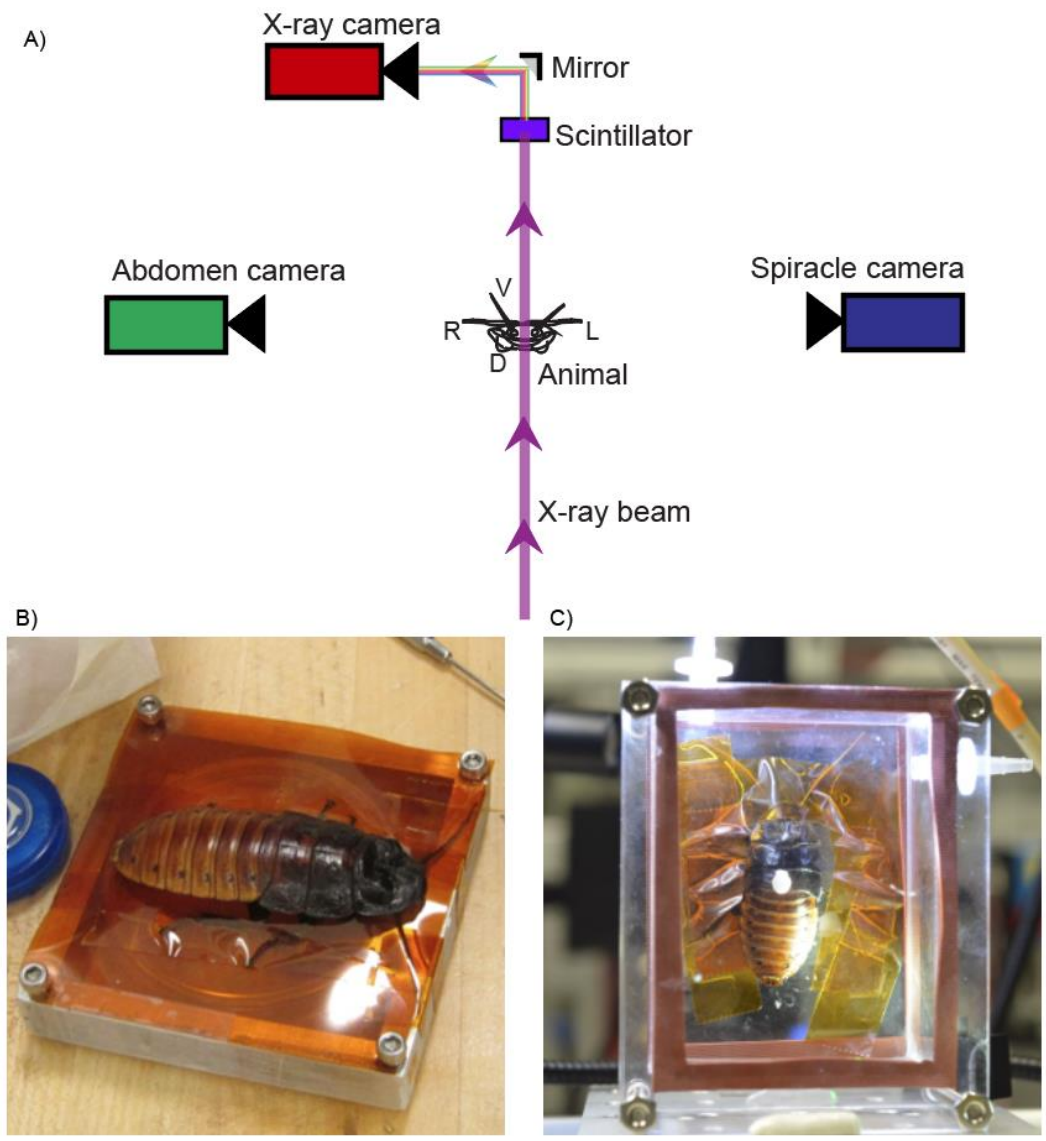


Figure 3: The setups used to record cockroaches. A: Top-down schematic demonstrating the camera setup used at the APS. The animal was mounted in the hutch using Kapton tape to secure its legs in a viewing platform. A video camera to the left of the animal was set up to record abdominal movement. A video camera to the right of the animal was set up to record between one and three abdominal spiracles. The synchrotron x-ray beam passed through the animal's dorsal side into a scintillator, where it was converted to visible light and recorded by a third camera, producing phase-contrast footage of the animal's internal structures. B: A male hissing cockroach restrained with Kapton tape on the observation frame. C: A male hissing cockroach restrained with Kapton tape in the environmental chamber.

Simultaneously with the internal x-ray video, external video of the abdomen and spiracles was captured using machine vision cameras (Pike, Allied Vision Technologies GmbH, Stadroda, Germany). The

abdomen was filmed using a 35 mm lens (Nikon Corporation, Chiyoda, Tokyo, Japan) at a distance of 0.5 m, with an image size of 448 x 728 pixels and with frame rate of 8 to 25 frames per second. Video of the spiracles was collected using a second Pike camera with a macro lens (Nikon 2.8 105 mm); this camera was anchored to the stage to ensure that the spiracle remained in frame as the insect was translated for positioning in the X-ray beam. Spiracle video was recorded with an image size of 600 x 500 pixels and a frame rate of 8 to 25 frames per second

The camera and specimen frame assembly were mounted to two stacked translation stages that enabled vertical and horizontal control of position in the x-ray beam. The two Pike video cameras were synchronized using MotionPro Timing Hub software (Integrated Design Tools, Tallahassee, FL) operating on a Macintosh Mini computer (Apple Inc., Cupertino, CA).

The external cameras were synchronized with the x-ray video post hoc using a pulse of light from an LED, triggered by an external voltage pulse (5 V, ~0.1s per pulse). The voltage pulse was routed to the audio input on the x-ray video tape recorder, producing a brief burst of sound with an identifiable audio waveform. The start of the sound pulse was then matched with the start of the light pulse to synchronize the footage. Nine cockroaches were tested, producing six hours of video; sequences disrupted by excess movement were not analyzed.

We noted no differences in respiratory behaviors associated with the animals' vertical orientation (paired t-test for means in abdominal frequency and amplitude, $p < 0.05$), allowing us to combine the data sets from the different experimental setups. Exposure to the X-ray beam for more than 12 minutes appeared to damage the function of abdominal spiracles, causing them to stop opening for many minutes at a time. Those portions of the data sets are not included in this analysis, and we attempted to avoid exposing the animals to harmful levels of radiation by limiting sequences to 12 minutes or less.

Video collection: Setup 2

In our second and third experimental sessions, we tested an additional 11 animals. For these recordings, the frame mount was replaced with a sealed acrylic chamber, which enabled more precise control over the environmental conditions. A gas mixture of 21% oxygen and 79% nitrogen was flowed into the chamber at 1 L/min. The exterior body movements were recorded using two video cameras: a HandyCam 4K (Sony Corporation, Tokyo, Japan) for the abdomen and HandyCam NEX-VG10 (Sony Corporation) with a macro lens (Nikon Sigma 180mm 1:2.8 APO Macro DG HSM) for the spiracles. Video was recorded at an image size of 720 x 480 pixels at 24 frames per second. The three cameras were synchronized post hoc using flashes of light inside the beamline hutch triggered by the external light switch. The X-ray video collection technique was used as before, except that the beam gap was increased to 24 mm to reduce potential radiation damage to the animals' tissue. We also limited x-ray exposure to a given spiracle to a maximum of five minutes.

Analysis of tracheal compression and internal spiracle state

To quantify internal tracheal compression, we manually identified the frames at which a tube began to collapse, was fully collapsed, began to re-inflate, and was fully re-inflated (Figure 4). A total of 93 tracheal compression events were quantified from seven specimens.

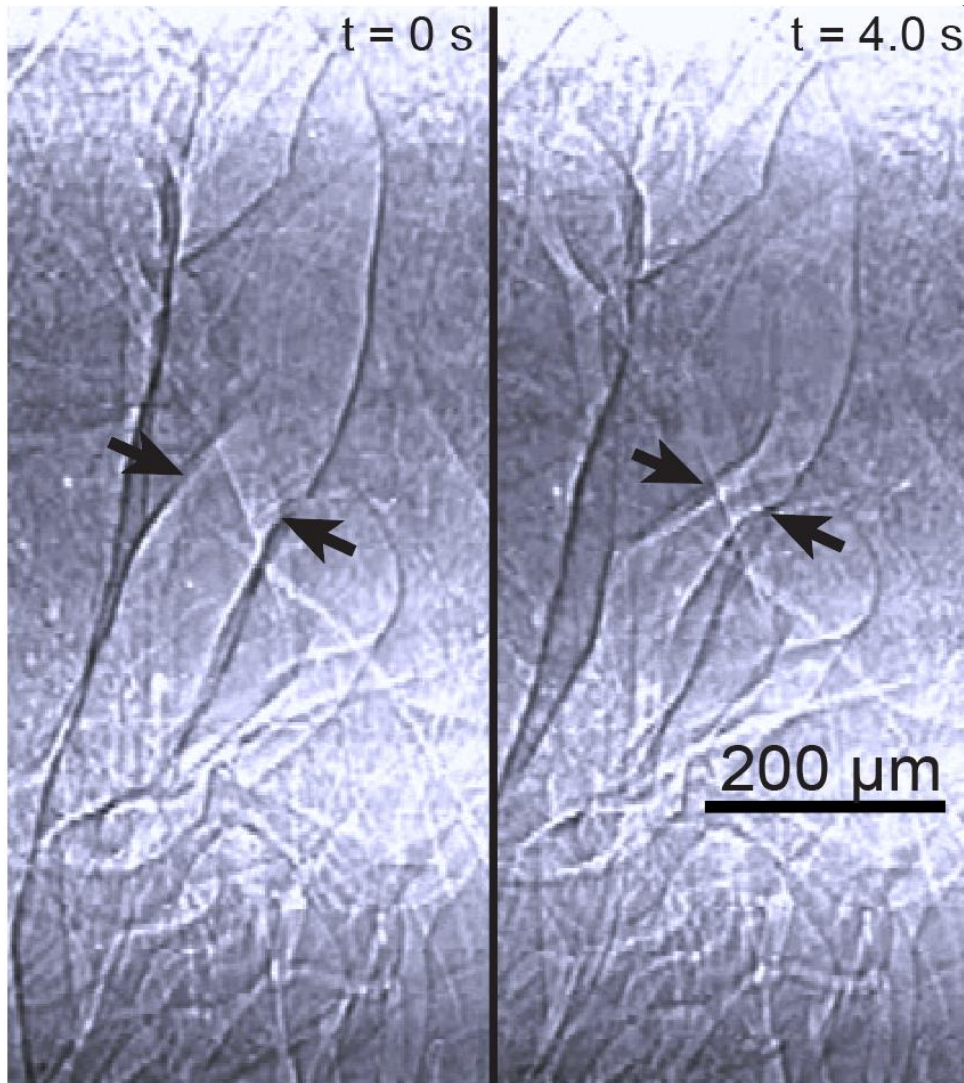


Figure 4: Manual frame-by-frame analysis was used to assess the state of tracheal collapse in phase-contrast x-ray video. Four possible states were scored: Fully expanded (shown on the left), initial collapse, full collapsed (shown on the right), and starting to re-inflate.

To quantify spiracle movement, we scored the following frames by visual inspection: frames at which the spiracle started to open, frames at which it appeared to be fluttering, the frame at which it became fully open, the frame at which it started to close, and the frame at which it was fully closed (Figure 6a); a total of 185 spiracle events from 14 specimens were quantified.

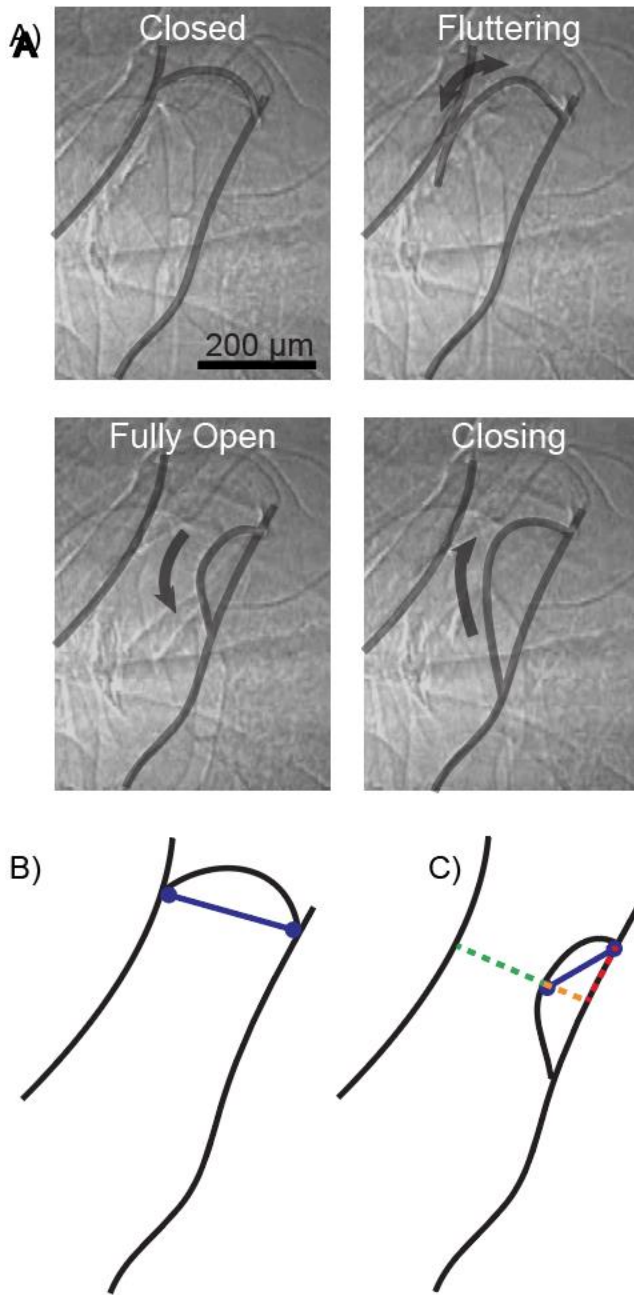


Figure 5: A: X-ray video frame of an abdominal spiracle demonstrating both fluttering and complete opening behavior. The image has been annotated for clarity. B: Technique for directly assessing the available area for flow through the spiracle manifold. A “default” state representing a fully closed spiracle is measured from the hinge of the spiracle flap to the opposite wall (blue line) C: As the spiracle moves through its opening arc, the line is redrawn to extend from the hinge to the point on the flap closest to the abdominal wall (blue wall). By comparing the length and angles of these two lines, it is possible to estimate the remaining area available for airflow (orange, red, and green lines).

Using a subset of these recordings, we quantified the kinematics of the spiracular flap using Fiji software (Schindelin et al., 2012) to estimate effective open diameter of a given spiracle, as well as the angle of the spiracle flap with relation to the adjacent manifold. These measurements were taken by drawing a line from the spiracle hinge to the point on the spiracle flap closest to the opposite wall (Figure 6b). A calibration grid (400 lines per inch) was used to convert pixel values into micrometers. We estimated the area open for airflow through the spiracle using the following equation:

$$A = \pi r^2 (R^2 - r^2)$$

where R is the radius of the spiracle manifold and r is the maximum radius occluded by the spiracle flap, assuming that the manifold and flap both have a circular cross-section. A total of 48 spiracle opening events from 9 animals was digitized using this process. To determine the measurement error associated with digitization, five different experimenters performed multiple measurement sets (Figure 7); these individual measurements were compared to the mean angle and radius measurement for each frame to calculate the average measurement error.

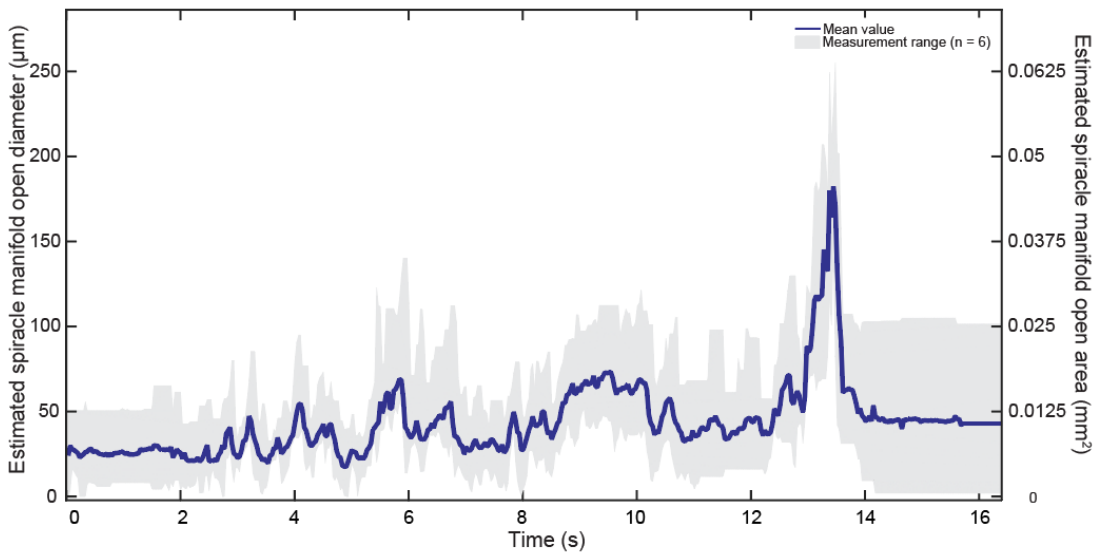


Figure 6: Measurement error associated with the manual tracking techniques detailed in Figure 5. Six different measurements were taken of the same sequence by a total of four researchers. The mean value is shown as the dark line, and the maximum and minimum measurement for a given frame are shown in gray.

Analysis of abdominal pumping

The abdominal movement footage was digitized semi-automatically using position tracking software (DLTv5 (Hedrick, 2008)). Points along the animal's dorsal midline at the intersections of the thoracic and abdominal tergites were tracked across video frames (Figure 2). These points were chosen because the tergites are rigid and visible in most specimens. The anterior edge of the second abdominal tergite, coinciding with the apex of the dorsal surface, produced the most consistent signals representing gross abdominal movement. We analyzed 155 minutes of video footage encompassing 861 pumping events.

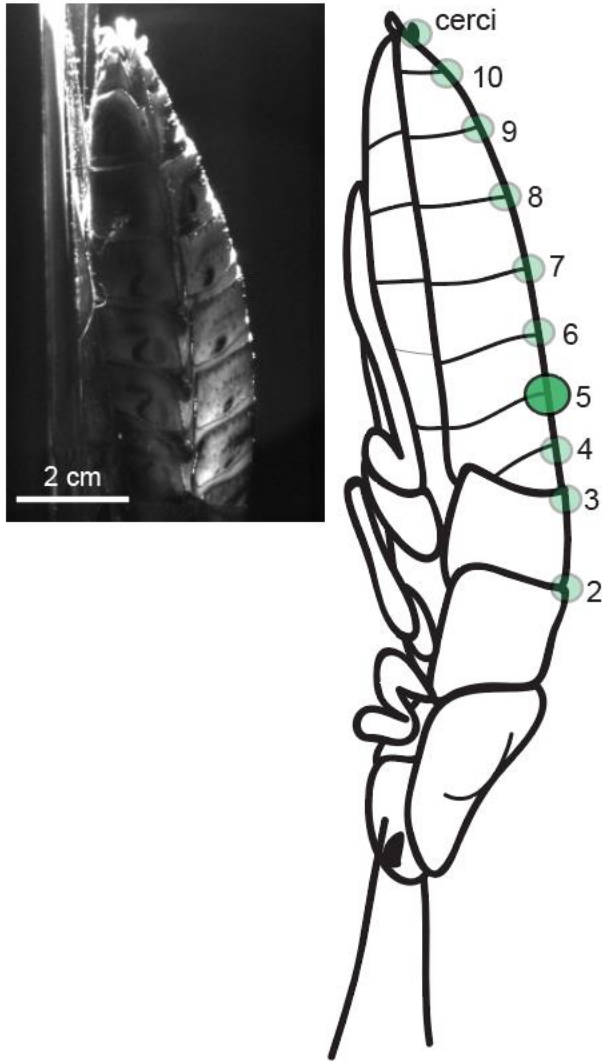


Figure 7: Diagram of the abdominal pump tracking method. DLT software was used to track points along the animal's dorsal side; the sum of their displacements represented the state of abdominal compression. The circles represent tracked points on the dorsal midline between abdominal tergites; the numbered labels refer to the nearest spiracle. Point #5, on the posterior edge of the fifth tergite and highlighted above, was chosen for analysis of abdominal pumping behaviors.

The digitized point locations were converted into millimeters with ImageJ (Schneider et al., 2012) using the previously measured length of the animal. Abdominal displacement magnitude was defined as the height of the point in the relaxed state to the height of the point in the compressed state. To compare among specimens, displacement magnitudes were normalized by body length. Average abdominal pump frequency was calculated by dividing the total number of pumps in each sequence by the duration of the sequence. Abdominal pump duration was calculated as the time between the start of abdominal compression and the time that the abdomen returned to the relaxed state.

Results

Video analysis revealed a correlation in timing of behaviors among abdominal pumping, tracheal tube collapse, and spiracular valving in the Madagascar hissing cockroach.

The average abdominal pump displacement was 0.24 ± 0.15 mm with a mean pump duration of 1.90 ± 0.95 s and a frequency of 0.10 ± 0.09 Hz. After normalizing by body length, we found a mean displacement during abdominal pumping of 0.47 ± 0.33 % of the body length.

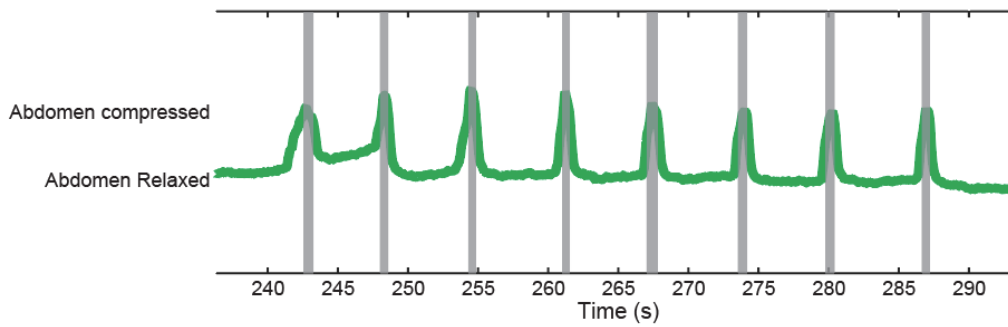


Figure 8: Correlation of tracheal compression with abdominal pumping. The green line represents the abdomen state (positive peaks show pumping events) and the gray bars indicate when the tracheal tubes are collapsed.

Specimen number	Mass (g)	Sex	Experimental setup	Tracheal events	Mean peak difference (s)	Mean start difference (s)	Mean end difference (s)
1	6.22	M	1	11	-158%±56%	178%±72%	-78%±178%
7	6.94	M	1	17	-13%±99%	79%±70%	-34%±131%
14	7.23	F	2	8	-5%±33%	14%±19%	-3%±60%
15	7.37	M	2	12	-20%±10%	58%±24%	-51%±0.23%
16	9.84	F	2	10	-19%±26%	112%±33%	-44%±34%
17	7.89	M	2	6	-77%±130%	57%±26%	-90%±53%
25	7.57	M	2	12	-43%±17%	23%±27%	-41%±0.29%
26	8.19	F	2	11	-7%±46%	85%±8%	215%±148%

Table 1: The behavior of tracheal tube events compared to abdominal pump events. The columns represent the difference, in relation to the entire length of the pump event, between the start of the pump and the start of tube collapse, between the peak of the abdominal pump and the peak of tube collapse, and between the end of the pump and the end of tube collapse.

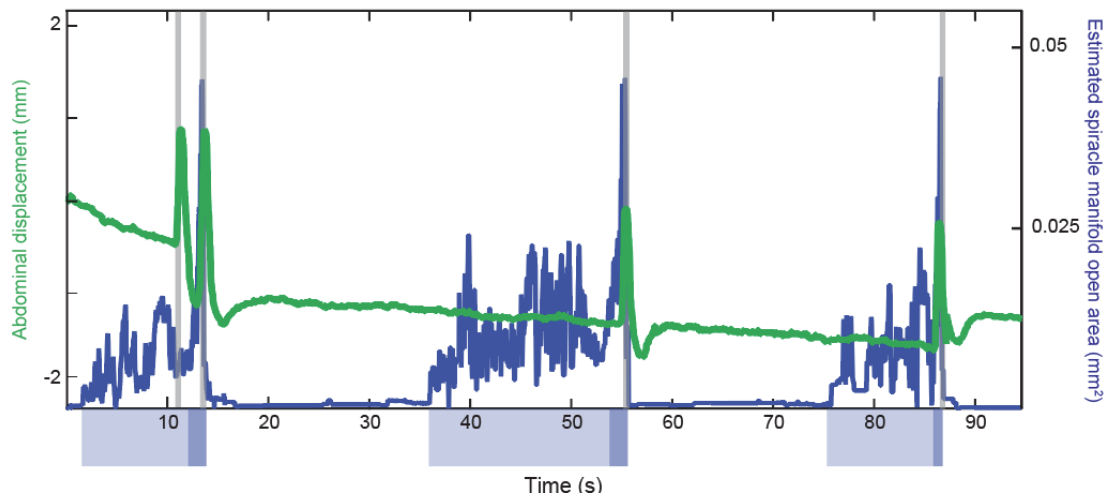


Figure 9: A sample diagram of all three behaviors acting in direct correlation. Abdominal pumping, tracheal collapse, and spiracle state are shown. Here we report the vertical displacement of the top edge of tergite #5. A positive peak represents an abdominal compression event. The estimated open area of the spiracle manifold is shown as a blue line. Tracheal collapse events are shown as gray bars. The blue bars below the x-axis correspond to early assessments of the spiracle in the fluttering state (light blue) or open state (dark blue).

There was no significant correlation (Student's t-test, $p > 0.05$) between abdominal pump displacement and pump frequency or duration. Pump frequency remained generally constant across the duration of any given sequence.

Tracheal collapse co-occurred with abdominal pumping. Tube collapse started 0.86 ± 0.70 s after the start of abdominal compression. Individual tracheal tubes were completely collapsed 0.01 ± 0.98 s

before abdominal compression peaked. Tubes returned to their relaxed state 0.34 ± 1.31 s before the end of abdominal compression.

We normalized the duration of each abdominal pump based on duration of the abdominal pump cycle to compare across separate events and specimens. Tube collapse started $32 \pm 22\%$ of the duration of abdominal compression after abdominal compression started. Individual tubes were completely collapsed $1.5 \pm 0.27\%$ and returned to their relaxed state $12 \pm 37\%$ of the pump duration before abdominal compression ended.

Discussion

Phase-contrast x-ray video allows us to clearly visualize the internal dynamics of the abdominal tracheal tubes in this animal. Across all observed specimens, abdominal tracheal compression occurred in close synchrony with abdominal compression, suggesting that abdominal pumping is responsible for tube collapse.

Abdominal pumping and tracheal tube collapse

The timing of abdominal pump and tracheal tube collapse events suggests a direct physical linkage between movement of the abdomen and collapse of the tracheal walls. The structure of the cockroach tracheal tube walls allows the tubes to collapse under pressure at specific points, driving advective flow through the system by displacement of volume (Socha & De Carlo, 2008; Socha et al., 2008; Webster et al., 2011). This indicates that the abdominal pump has a respiratory function and assists in driving advective flow (Weis-Fogh 1967, Harrison 2003).

Coordination between abdominal pumping and spiracular valving

The coordination of abdominal pumping and the spiracle open phase observed in this study is consistent with previous findings (Heinrich et al., 2013). This data also correlates well with existing literature that suggests active opening of the abdominal spiracle structure is coupled to the same nervous architecture that controls abdominal pumping (Nelson, 1979). Under normoxic conditions, during periods of active respiration (i.e. repeated abdominal pumping motions within a short time frame), the spiracles can be observed to open fully at the start of abdominal compression, and close again before the abdomen begins to relax. Each abdominal pump is typically accompanied by a brief period of fluttering in which the spiracles partially open and close at high frequency (>15 Hz) (Figure 6).

Internal spiracle dynamics

The use of phase-contrast X-ray to study the internal spiracle dynamics represents a useful approach to understanding the mechanics of this flow system. Spiracular valving behavior has been previously studied for *G. portentosa* (H. L. Contreras & Bradley, 2010) but the precise dynamics of the individual spiracle have not been studied at this level of detail. Careful analysis of the spiracle movement using phase-contrast x-ray revealed important details about the specific kinematics of spiracle movement, both during the fluttering phase and during the transition to full openness.

The angle and movement of the spiracle dictates the behavior of gas flow both during and between pumping, so an accurate estimate of the effective cross-sectional area available for flow is important for understanding the fluid dynamics of gas exchange in the insect model. If the spiracular manifold can be modeled as a cylindrical pipe, then the area available for gas flux is the difference between the cross-sectional area of the spiracle manifold and the cross-sectional area obstructed by the spiracle flap, and the animal can modulate gas exchange by opening and closing the spiracular valve. In general, depending on the specific spiracle and the size of the animal, the area available for flow is 0 μm^2 when the spiracle is closed, 95% of the manifold area when the spiracle is fully open, and between 0% and 60% during the rapid spiracular flap oscillation of the flutter phase. However, given that the fluttering frequency may be higher than our available measurement rate (30 Hz), future studies may reveal more complex dynamics.

Our calculated values for the area of the manifold open to flow corresponds well to existing knowledge about spiracular conductance. Measures of conductance performed via respirometry have identified clear phases of differing conductance that are reflected in our video estimations of spiracle manifold area (Hetz & Bradley, 2005).

One interesting observation is the similarity of the pattern of spiracle opening present during active respiration (Figure 9) to the CO_2 emission patterns found during discontinuous gas exchange, albeit at the second scale instead of the minute scale (Heidy L. Contreras et al., 2014; Heinrich et al., 2013). This suggests that a similar control mechanism for modulating gas exchange exists during both types of respiratory patterns. We believe that these results indicate a consistent pattern of airflow exchange utilizing a diffusive step during the flutter phase, and then an advection on the timescale of the tube collapse, assuming all the tubes are collapsing simultaneously.

Conclusion

X-ray visualization allows for a direct analysis of the physical dynamics of abdominal spiracle movement. By measuring the precise movement of abdominal spiracles, we can better understand and identify the various movements associated with spiracular respiration, including a more direct and objective definition of the fluttering state commonly reported in insect respiration literature. Using this information, we can begin to develop new hypotheses about the fluid dynamics of airflow moving into and out of the system. Future work in simulated models can be used to develop and test new hypotheses about metabolic adaptations in insects and similar systems

Chapter 2: The insect's response to hypoxia and hyperoxia

Introduction

Many animals can modulate frequency and amplitude of their breathing behaviors in response to increased metabolic demand or decreased availability of oxygen. An animal may be exposed to a range of oxygen conditions as it makes its way through different environments (Hoback, W.W.; Stanley, 2001; Parker & Smith, 1990; Schmitz & Harrison, 2004) or responds to varying metabolic conditions (Komai, 1998). An insect can compensate for different environmental oxygen concentrations or oxygen demands by modulating its respiratory behaviors to drive flow according to its needs (H. L. Contreras & Bradley,

2010; Kinnamon et al., 1984; Komai, 1998; Lighton, 1988). These strategies can be observed in all life stages and can take advantage of both diffusive and advective airflows, in both active and discontinuous breathing patterns (Simelane et al., 2016).

The Madagascar hissing cockroach (*G. portentosa*) is a leaf litter-dwelling insect. The animals have three basic respiratory tools at their disposal: the amplitude of their abdominal compression, the frequency of their abdominal compression, and their total spiracular conductance. The cockroach maintains a temporal coordination between external abdominal movement and the collapse of internal tracheal tubes, and links this tracheal actuation with spiracular valving to drive a net unidirectional flow of air in through the thoracic spiracles and out of the abdominal spiracles (Heinrich et al., 2013). Previous studies have identified a link between CO₂ output and tracheal abdominal compression (Pendar et al., 2016). However, these behaviors may not change linearly with the available oxygen (Simelane et al., 2014).

Here, we examine how the animal changes its abdominal pump amplitude and frequency in response to varying environmental oxygen concentrations. This behavior allows it to manipulate the volume of the tracheal network and potentially drive flow at different rates as oxygen supply changes. We apply phase-contrast x-ray imaging to directly visualize the internal respiratory structures of an actively respiring insect.

We also explore how spiracle control behavior changes, especially regarding time spent during the closed, open, and fluttering phases. Here we hypothesize that the insect will attempt to increase spiracular conductance when exposed to low oxygen concentrations in order to increase overall gas exchange.

Finally, we examine how the relationship between the spiracle state and abdominal pump changes against varying oxygen concentrations. We hypothesize that the animal would attempt to optimize its advective and diffusive respiratory flow patterns to compensate for limited oxygen availability and the metabolic costs of employing active pumping.

We hypothesize that in hypoxic environments, the insect will increase its overall respiratory conductance by increasing the frequency of its abdominal pump and the comparative amount of time the spiracles are left open. Conversely, in environments rich with oxygen, the animal will attempt to conserve energy and reduce water loss (Simelane et al., 2014) by limiting the frequency of its abdominal pump and the amount of time that the spiracles remain open (Vrtar et al., 2018). These findings will fill in a valuable gap in our knowledge about how organisms make behavioral tradeoffs to maintain homeostasis as resources and demands change.

Methods

We used phase-contrast x-ray imaging to visualize the internal respiratory structures and behaviors of adult Madagascar hissing cockroaches while they were exposed to a range of hypoxic and hyperoxic conditions in a sealed acrylic chamber. Five adult animals (3 male, 2 female) were studied in sequences lasting 10-12 minutes. Each animal was given 5 minutes to acclimate to the new oxygen concentration

before video collection began. We collected our videos at the Argonne National Laboratory at beamline 32-ID, with a beam energy of 25 keV and a gap of 24 mm. Video was collected at 30 frames per second with a resolution of 720 x 480 pixels. The x-ray video collection methodology is explained in more detail in Chapter One.

Experimental Setup

The animals were secured head-up to a transparent acrylic plate (1/8" thickness) by Kapton tape applied to their thorax and legs. This plate was attached with metal screws to the rest of the environment chamber and sealed with rubber gaskets. Gas was introduced to the chamber through a 9 mm port on the top of the chamber; gas flowed out of the chamber through another identical port on the lower right.

The animal was placed in an acrylic chamber in the center of a metal beam. Its legs were restrained with Kapton tape and its head and thorax were restrained with gaffer's tape. A video camera was mounted on each end of a metal beam affixed to the translation platform and aimed at the animal's abdomen and spiracles. These videos were collected at 24 frames per second. The x-ray beam passed through the dorsal side of the specimen and into a scintillator where it was converted into visible light and captured by a third camera. Each sequence lasted approximately 10 minutes.

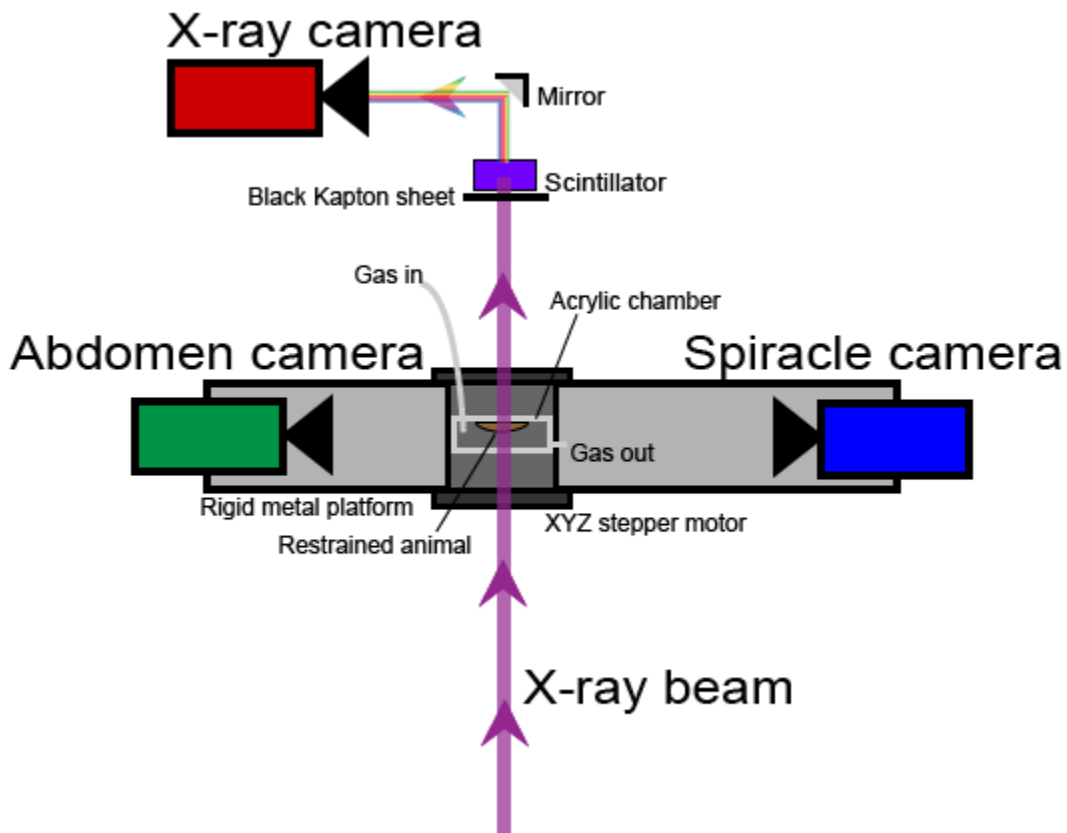


Figure 10: Diagram of the imaging and respiratory gas exchange setup at the Advanced Photon Source beamline.

Oxygen Control

Nitrogen and oxygen were mixed using a Sable Systems MFC-4 mass flow controller (Sable Systems, North Las Vegas, NV) to attain the desired oxygen concentration at a flow rate of 1 L/min. Before beginning data collection on each trial, the output oxygen concentration was confirmed using a separate measurement device (OxyCheq O₂ Analyzer, OxyCheq, Marianna, FL) affixed to the outlet port. Oxygen concentrations of 3%, 5%, 10%, 21%, and 30% were used, balanced with nitrogen. The animals were exposed to each oxygen level for approximately 5 minutes before data collection began.

Video Digitization

We used DLTv5 (Hedrick, 2008) to digitize movements of the external abdominal tergites. Specifically, by tracking points on the dorsal surface of the abdomen on the edge of as many tergites as were reliably visible in each video sequence. This method is explained in more detail in Chapter One.

Spiracle state was assessed manually using two methods, both drawing from x-ray video footage of the spiracles. For 24 sequences, spiracle state was scored on a frame-by-frame basis according to when the spiracle started to open, was fluttering, transitioned from fluttering to open, was open, and started to close. This method is explained in more detail in Chapter One.

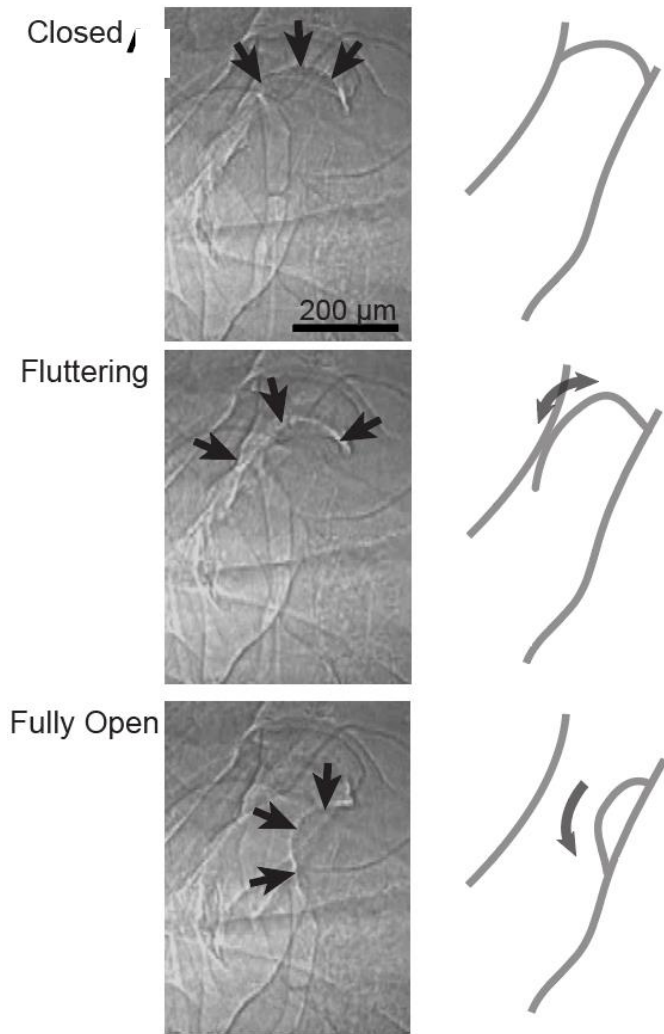


Figure 11: Manual scoring of spiracle state. Spiracle state was assessed frame by frame as either closed, fluttering, or open.

For a smaller subset of 5 sequences, the spiracle state was assessed with ImageJ. In each frame featuring the spiracle, a line was drawn from the spiracle's chitinous hinge to the opposite wall of the spiracular manifold. The length and angle of this line was recorded and used to estimate the total open area of the spiracular manifold, assuming a circular cross-section. This process is explained in more detail in Chapter One.

Due to the nature of the x-ray techniques used to visualize internal structures, an individual animal could only be studied for a limited time (less than 10 minutes) before radiation damage started to effect essential tissues.

Results

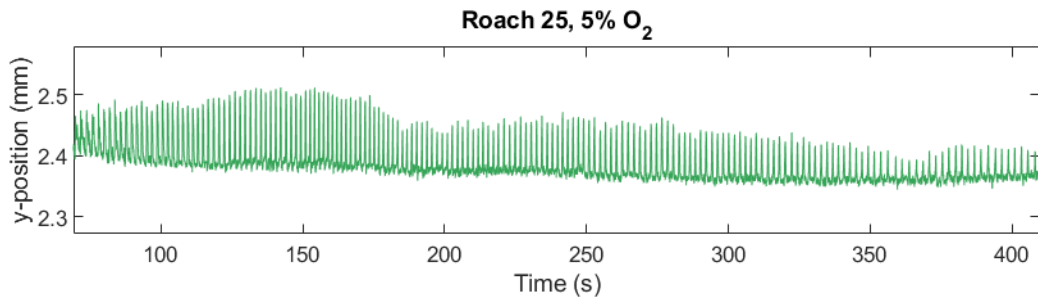


Figure 12: A representative trace of abdominal movement. Regular abdominal pumps are clearly visible as peaks in the tracked y position of the edge of tergite 5. There is a slight change in pump amplitude throughout the sequence as well as a minor shift in pump frequency. The change in baseline is due to the animal shifting position during the sequence. See Appendix A for more abdominal state sequences.

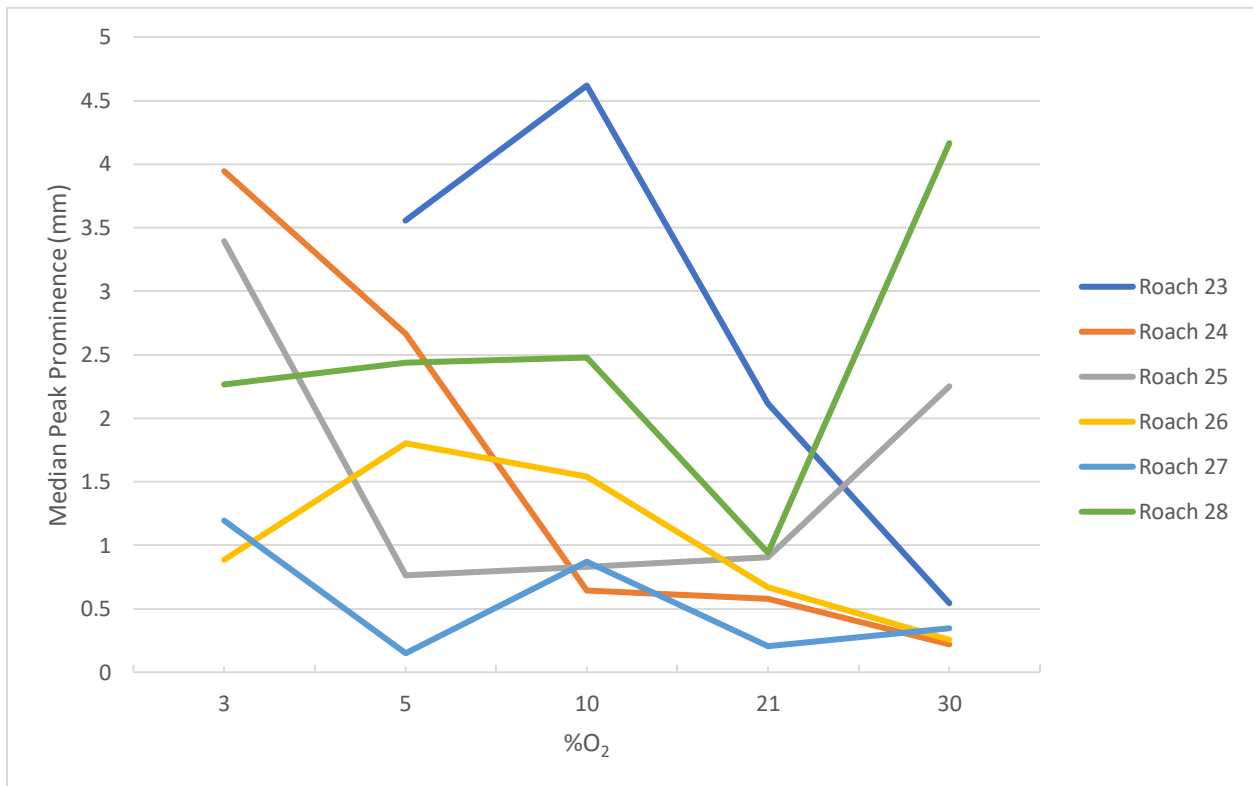


Figure 13: The median abdominal pump amplitude for each roach at each O₂ concentration. There is no clear trend regarding pump amplitude vs hypoxia or hyperoxia, either at the level of the individual roach or across all specimens, suggesting that the animals do not compensate for hypoxia or hyperoxia by adjusting the amplitude of their abdominal pumps.

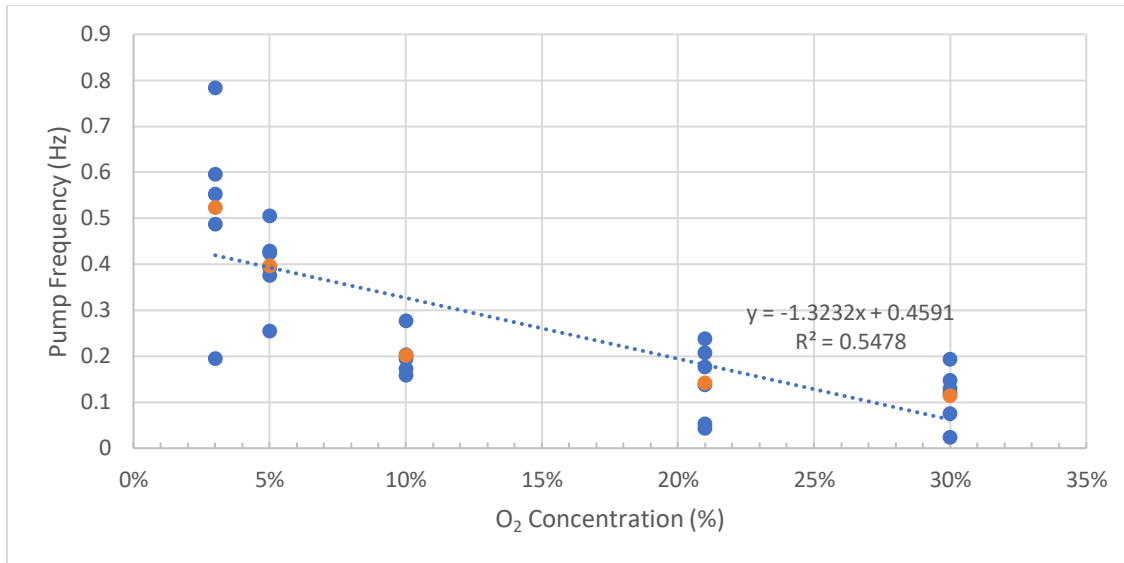


Figure 14: Abdominal pump frequency vs oxygen concentration, averaged across all specimens. Each point represents the average abdominal pump frequency across an entire sequence for a given animal at a given oxygen concentration. The orange dots represent the mean abdominal pump frequency for all animals at a given oxygen concentration, with the black bars representing one standard deviation. As oxygen concentration decreases, pump frequency increases. The dotted line represents a linear fit. These data suggest that the animals increase their abdominal pump frequency in response to hypoxia, and decrease their abdominal pump frequency in response to hyperoxia.

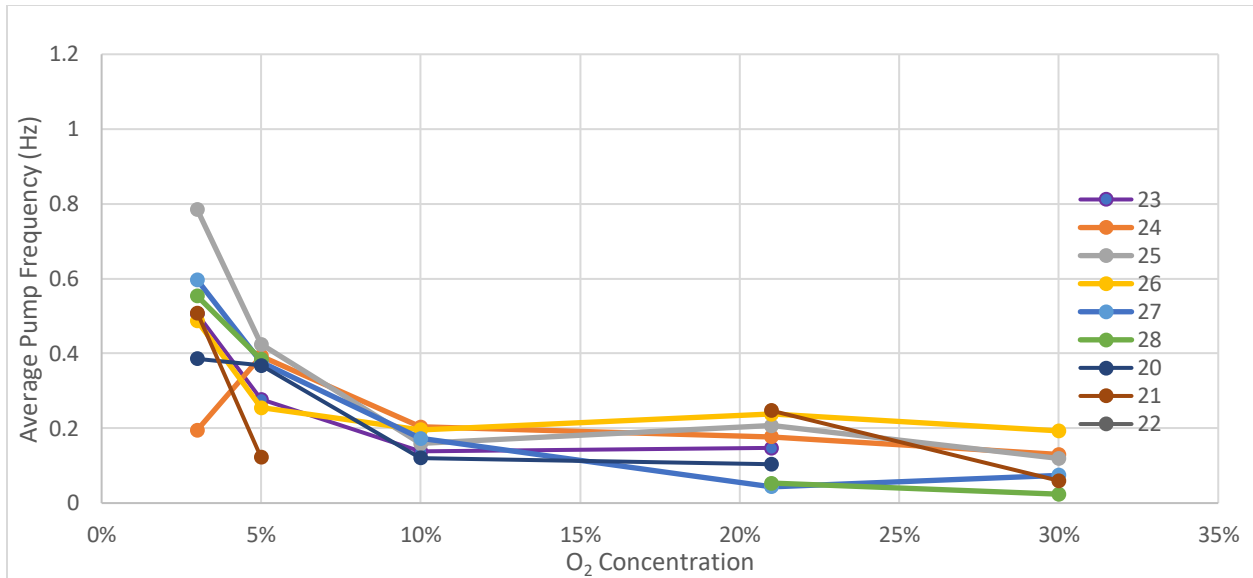


Figure 15: Abdominal pump frequency vs oxygen concentration, plotted per insect. While we see a clear trend toward increasing abdominal pump frequency at very low oxygen concentrations, there is a less obvious trend between 10% and 30%.

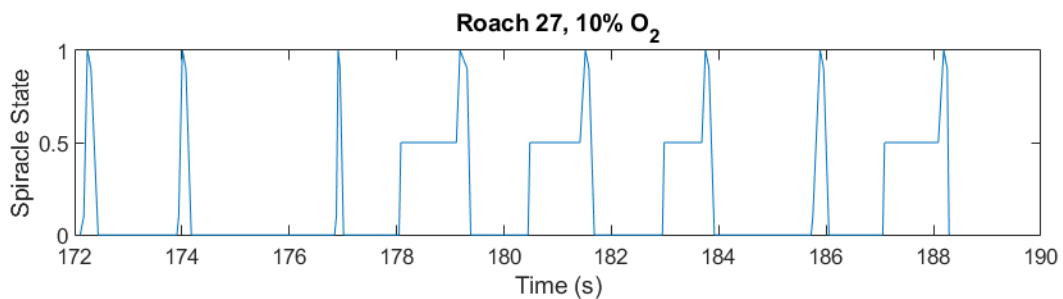


Figure 16: A representative trace of spiracle state versus time for a single insect. A value of 0 means that the spiracle is fully closed and a value of 1 means that the spiracle is fully open. A value of 0.5 represents spiracle fluttering. A pattern of closed-fluttering-open is clearly visible for half of the sequences. The remaining events do not feature fluttering. See Appendix B for more spiracle state sequences.

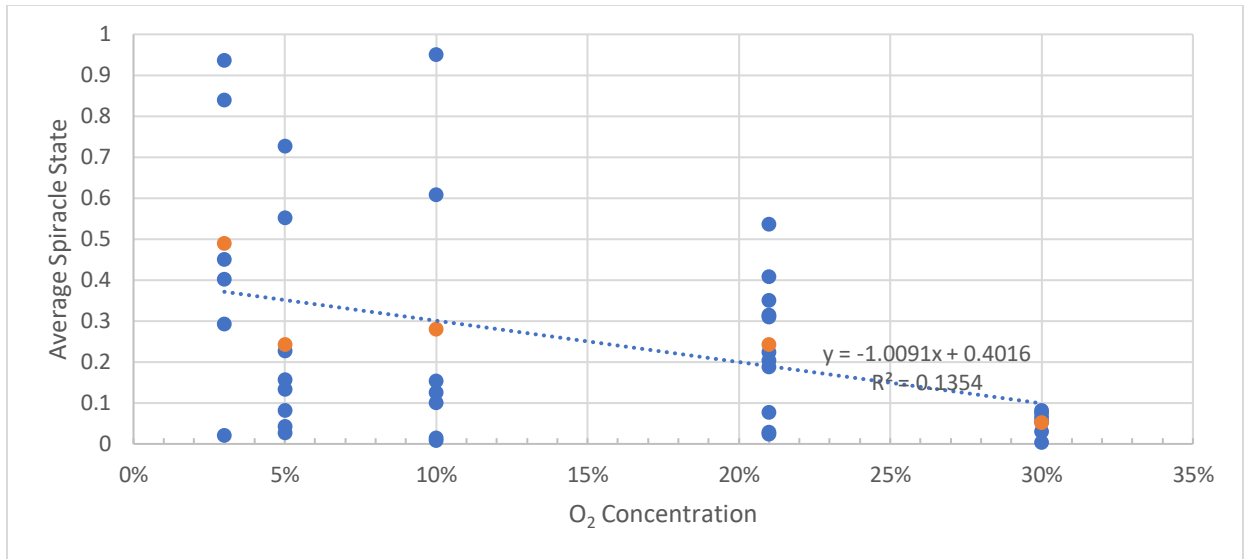


Figure 17: Average spiracle state vs oxygen concentration. Values of spiracle state range from 0 to 1, with 1 representing a fully open spiracle, 0 representing fully closed, and 0.5 representing fluttering. These values were calculated based on a manual frame-by-frame scoring of the spiracle state across the entire sequence. Each dot represents this calculated value for a given sequence. The orange dots represent the mean openness for that oxygen concentration across all animals. The dotted line represents a linear fit to the data. There was a significant increase in spiracle openness (compared to normoxia) at 3% O₂, and a significant decrease in spiracle openness at 30% O₂.

There was no significant change in abdominal pump frequency when animals were exposed to oxygen concentrations from a range of 10% to 21%. At a hyperoxic concentration of 30% O₂, abdominal pumping became significantly (Student's t-test, $p < 0.05$) slower. At the hypoxic conditions of 3- 5% O₂, abdominal pumping became significantly (Student's t-test, $p < 0.05$) faster. Abdominal pumping is directly linked to tracheal tube compression, so a higher pump frequency results in increased advective flow through the tracheal trunks.

Discussion

We found that the Madagascar hissing cockroach responds to hypoxia and hyperoxia by modulating the frequency of its abdominal pumping and the amount of time that the spiracles are open. Abdominal pumping has been linked to tracheal tube compression (see Chapter One), which is responsible for the creation of advective airflow in the larger tracheal tubes (Pendar et al., 2015, 2016, 2019). Combined with spiracular valving, a higher frequency of tracheal tube collapse drives more advective airflow through the tracheal network (Kinnamon et al., 1984), allowing airflow to be controlled according to metabolic needs and environmental conditions.

The spiracles do not remain open continuously and tend to stay closed at higher oxygen concentrations (greater than 21%). This is consistent with hypotheses regarding an insect's attempts to minimize water loss through the spiracles (Simelane et al., 2014) and oxygen toxicity (Hetz & Bradley, 2005). By increasing the frequency at which the tracheal tubes compress, more advective flow can be created in

tracheal network, driving greater volumes of gas through the system (Greenlee et al., 2014). In low oxygen environments (less than 10% O₂), this has the benefit of making more oxygen available overall for diffusion into the tissues. In high oxygen environments (greater than 21% O₂), less airflow is needed to deliver the same amount of oxygen to the tissues, so energy can be saved by minimizing the use of the abdominal muscles.

While the external patterns of abdominal pumping and spiracular valving in *G. portentosa* have been studied before (Heinrich et al., 2013), no research has been done on the internal spiracle dynamics or the response to hypoxia and hyperoxia. Given what we know about the link between abdominal pumping and tracheal tube compression (see Chapter One), here we identified pumping and valving mechanics on a sub-second temporal scale and examined the internal dynamics of tracheal compression and spiracular valving at the micron level, allowing us to specifically identify respiratory patterns during active ventilation.

We know from our experiments under normoxia in Chapter One that in *G. portentosa* abdominal pumping is directly linked to tracheal tube compression. Specifically, we know that the full tracheal tube compression cycle, from collapse to reinflation, of larger tracheal tubes happens within the cycle of an abdominal pump. Abdominal pumping was also linked to spiracular activity. When the abdomen is relaxed, the spiracles are closed. Just before the abdominal pump, the spiracles begin to flutter. When the abdomen pumps and the tracheal tubes are fully compressed, the spiracles open (see Figure 9, Chapter One).

Here we see the same pattern repeated at higher and lower frequencies of abdominal pumping, with modifications to how much time is spent in the flutter phase prior to the abdominal pump and the open phase. At higher oxygen concentrations, the spiracles spend less time in the flutter phase. At lower oxygen concentrations, more time is spent in the flutter phase. Given what we know about gas exchange patterns in the insect respiratory system (Pendar et al., 2015), these results suggest that advective flow happens in the tracheal system when the abdomen pumps and the tracheal tubes collapse (Tartes et al., 2000) and the tracheal tubes compress while the spiracles are open. Diffusive flux across the spiracles happens when the spiracles are fluttering and the abdomen is not pumping (Wasserthal & Frohlich, 2017). Behavioral changes enable the animal to adjust its rates of advective and diffusive flow according to the amount of oxygen available in the environment.

To our knowledge, no studies have been performed on the response to hypoxia and hyperoxia in the Madagascar hissing cockroach. The hissing cockroach exhibits two different mechanisms in response to changes in environmental oxygen concentration: adjusting the frequency of abdominal pumping and modulating spiracle state. This suggests that there may be considerable variation in the amount of available oxygen in their habitats and they are equipped to compensate accordingly (Schmitz & Harrison, 2004). This is consistent with hypotheses about the minimization of water loss through the spiracles (Lehmann, 2001; Simelane et al., 2014), oxygen toxicity to the tissues (Hetz & Bradley, 2005), and the metabolic cost of active respiration (Harak et al., 1996). These changes in respiratory behavior seem to be most pronounced at very high (30%) and very low (3%) oxygen concentrations, with less change from normoxia noted at 5% and 10% O₂. This suggests a rather wide range of “normal” oxygen

concentrations under which the animal does not need to change its behaviors to perform adequate gas exchange. This is consistent with evolutionary theories about insects developing adaptations for extreme conditions (Hoback, W.W.; Stanley, 2001; Kinnamon et al., 1984).

Future studies should incorporate flow-through respirometry and internal pressure measurements to better understand airflow patterns and the mechanisms of tracheal tube compression.

Chapter 3: A computational fluid dynamics simulation of the insect respiratory system

Introduction

Though much is known about the insect respiratory system, its intrinsic features present several challenges for direct study. It is generally very small, located almost entirely beneath the exoskeleton, and has highly complex network structures (Harrison, 2009). This system is capable of producing a net unidirectional advective flow to aid gas transport at the tissue level, moving fluid in through one set of spiracles and out through another to complement diffusive flux with advective gas exchange. Previous work has been largely focused on direct observation of external structures and behaviors (Heinrich et al., 2013; Pendar et al., 2016), or direct measurement of internal pressures and indirect measurement of bulk flows (Pendar et al., 2015). This allowed researchers to identify some flow creation patterns – such as microfluidic unidirectional flow - but not necessarily how the insect respiratory mechanisms created those patterns. Here, we have created and tested a simulated model of a generalized insect respiratory system in order to parametrically assess how its various features contribute to the characteristics of flow within the system. With this tool, we were able to test hypotheses about unidirectional flow creation and diffusion that could not be easily studied in a live insect.

A computational fluid dynamics approach to understanding the insect respiratory system represents an appealing method of assessing the effects of various respiratory parameters – tracheal geometry, valving and pumping patterns- in a system that may not be easily understood using experimental or analytical techniques. There are enough components present in the system that their interactions cannot necessarily be predicted.

In this study, we assessed how pumping schema, channel geometries, and valving properties affected flow rate, flow direction, and diffusive flux. Though some of these flow patterns may be simple enough that they can be calculated using fluid mechanics equations, there are enough parameters in effect that a more holistic study using computer simulations is necessary to develop an appropriately thorough understanding of the system.

Previous work

Previous systematic exploration neglected to incorporate the effect of spiracles, the muscularly-valved openings that connect the tracheal system to the external environment. The actuation of these organs is known to be closely associated with both the abdominal pump and local carbon dioxide sensors (Heymann & Lehmann, 2006; Lighton, 1973). It has been hypothesized in previous works that the action of the spiracles in concert with the abdominal pump is essential for the creation of unidirectional flow (Heinrich et al., 2013); movement of the abdominal pump – and thus tracheal tube compression (see Chapter 1) - is closely linked to spiracle activity to drive unidirectional airflow in through the thorax and out through the abdomen. Here, we use the simulated system to test the hypothesis that spiracular valving is required to produce a net unidirectional flow.

A report by Simelane et al (Simelane et al., 2014) models the entire tracheal system, including the spiracles, as an abstract mathematical network representing one or more flexible compartments. This model incorporates a great deal of specific physiological and chemical parameters from the insect system and provides a mathematical analysis of the tracheal network. However, in treating the system as a single flexible compartment, specific attributes of the network geometry are washed out, and it becomes impossible to see some of the smaller-scale properties of flow within the system. This study endeavors to observe how parametric adjustments to different aspects of the network geometry affect flow at specific points as well as in the system as a whole.

Methods

We used COMSOL Multiphysics 5.4 software (COMSOL, Inc., Los Angeles, CA) to construct and analyze a model that incorporates several key features of the insect respiratory system: the tracheal tube geometry, actuation via internal tube collapse, and abdominal spiracular valving. The system was constructed such that these features could be varied parametrically and independently.

Insect	Model	Parameters
Tracheal network	Channel geometry, transport of dilute species	Branching parameter, compartment ratios, length-to-width ratio
Spiracles	Valved outlets	Valve phase, duty cycle
Collapsible tracheal tubes	Internal sinusoidal pressure	Frequency, offset

Table 2: Parameters used in the simulated insect respiratory system. In order to test the effects of different physiological parameters, different aspects of the simulated tracheal network were varied parametrically for a range of physiologically relevant values.

Parameter	Values Tested
Branching parameter	0.5 – 1.5 at intervals of 0.25
Compartment ratio	0.7 – 1.3 at intervals of 0.3
Length-width ratio	3 – 1000 at intervals of 25
Valve phase	0 – 2π at intervals of $\pi/8$
Duty cycle	0 – 100% at intervals of 10%
Frequency	0.1 – 2 Hz at intervals of 0.1 Hz
Pump amplitude	40 kPa
Actuation offset	0 – 2π at intervals of $\pi/8$

Table 3: Parameter values tested. Throughout the course of the study, parametric sweeps were performed using the above values for each of the parameters listed in Table 1. Different values of the parameters were swept through to build a solution space that allowed us to identify how the parameter affected flow rates.

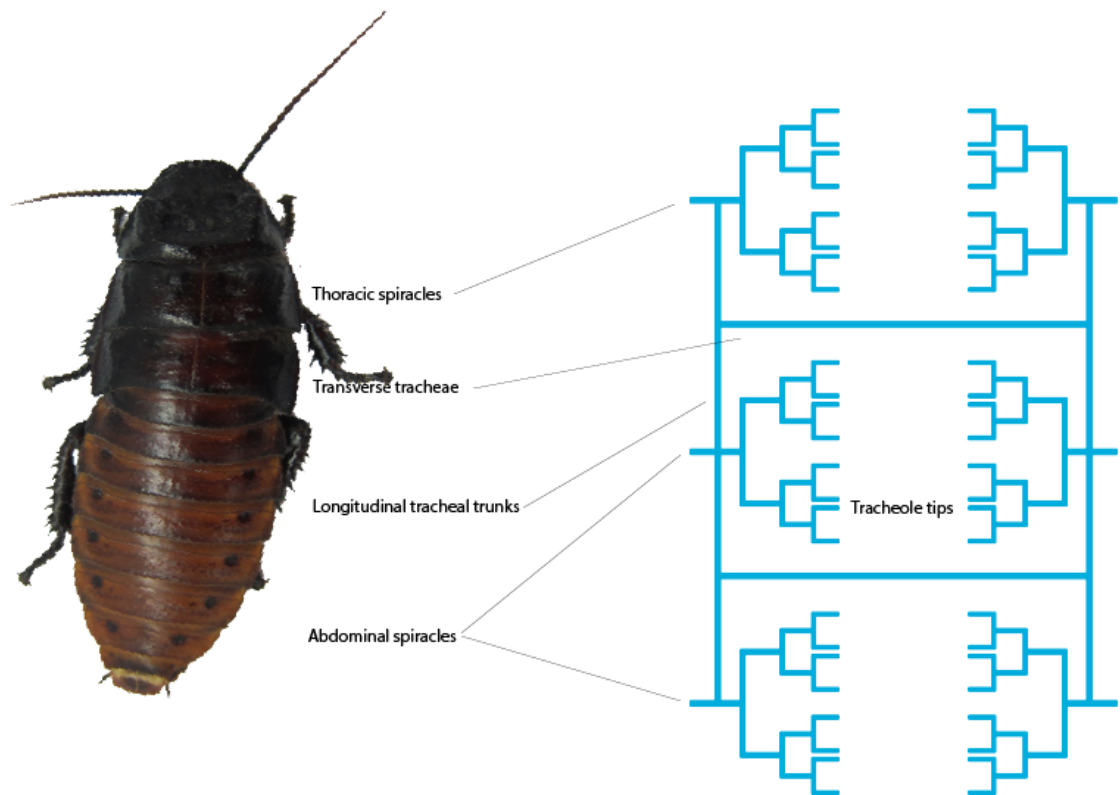


Figure 18: A model of the insect respiratory system. To build a simulated insect respiratory system, three “chambers” comprising three generations of channels were constructed and connected.

The tracheal network was split into three segments: anterior, central, and posterior. The three branching generations of tracheal tubes descended in diameter according to a branching parameter $X = d_0^2/2d_1^2$. The model allowed us to parametrically vary the relative sizes of the anterior and posterior segments (the central segment remained fixed). The ratio of channel length to width was also varied parametrically.

Though the insect respiratory system does not incorporate 90-degree angles at branching points, this simulation includes rectangular channels for two reasons: First, this approach made it possible to quickly and easily parameterize the channel geometry, such that we could make rapid and systematic changes during analyses. Secondly, this sort of channel geometry more closely approximates the typical construction of physical microfluidic devices, enabling to potential to more quickly translate findings from this study into applied engineering.

Though this simulation is intended to test hypotheses regarding the insect respiratory system, most of the experiments were carried out using water-filled tubes, rather than air. This decision was made to reduce computational complexity. However, the actuation pressure was correspondingly increased, resulting in flow in the same Reynolds number regime (~ 1) and allowing comparison back to the natural system.

Actuation of the tubes took place by applying a sinusoidal 40 kPa boundary condition in the fluid domain to the first-generation tubes in the central and posterior sections of the network. This pressure was applied across the entrance plane of the tubes in the axial direction pointing into the tubes. This was intended to simulate compression of the larger-diameter tubes in the insect respiratory system. For some experiments, the posterior tubes had their actuation offset by a parametrically-varied phase offset, in order to test the effects of a peristalsis-like pumping pattern.

Spiracular valving was mimicked by increasing the viscosity of fluid at the central and posterior ports with a square wave whose magnitude ranged from the viscosity of water (the fluid used in our simulations) to 10^5 Pa*s. This technique was adapted from a tutorial video on the COMSOL website (<https://www.comsol.com/video/simulating-closing-gate-valve-part-1>). The valving happened at the same frequency as the sinusoidal pressure actuation, set out of phase at various values from $0 - 2\pi$ radians, and with a duty cycle ranging from 0% (off all the time) to 100% (on all the time). See Table 3 for more details.

The second part of our study incorporated the addition of a diffusive flow component. The “transport of dilute species” module was added and bound to the laminar flow module. This allowed us to study the effects of different parameters on the creation of diffusive flux at different points in the system, with the goal of identifying the relationship between diffusive and advective flux. We used the diffusivity constant of carbon dioxide in air (10 cm²/s) to model diffusive flux in an insect system. Here we also began to vary the ratio of length vs width in the network. In our advective flow studies, this value was fixed at 10. For our studies that incorporated diffusive flux, we increased this ratio at various increments all the way up to 1000, representing very long and thin tubes (see Table 3).

Results

When internal channels are actuated with a symmetric sinusoidal pressure pulse, unidirectional flow can only be produced via coordinated spiracular valving action. Further, the specific temporal parameters of the valving cycle dramatically influence flow direction and velocity.

Network geometry alone cannot influence the production of bulk unidirectional flow. When there are no valves, a sinusoidal pressure actuation produces a sinusoidal pattern of flow through the system, with no net flow out the posterior or anterior segments over the course of one pump cycle. Even adjusting the hydraulic resistance of the chambers such that, for instance, there is less resistance to flow in the posterior segments does not influence the net direction of flow.

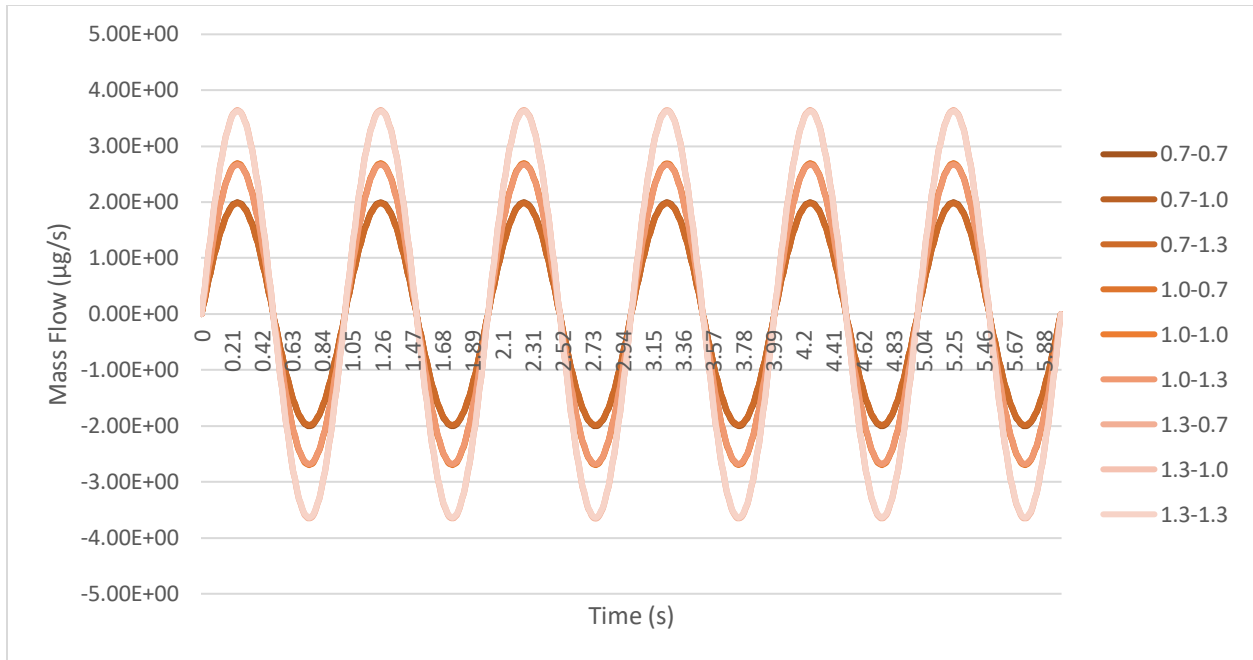


Figure 19: The effect of channel size on mass flow rate. Each shade of orange here represents a combination of differently sized anterior and posterior channel segment ratios.

There is no net flow at any combination of channel ratios. Flow is entirely sinusoidal, but some ratio combinations are better at allowing more net flow, based on the hydraulic resistance of the channels.

Only by adding valves at the simulated abdominal spiracles allows for a net unidirectional flow. Moreover, there is an optimal duty cycle of 50% on at which unidirectional flow is produced. This effect is most pronounced in the posterior direction when the valve phase is offset from the pump phase by π radians. Conversely, unidirectional flow in the anterior direction, out through the thoracic spiracles, is maximized when the valve phase is not offset from the pump.

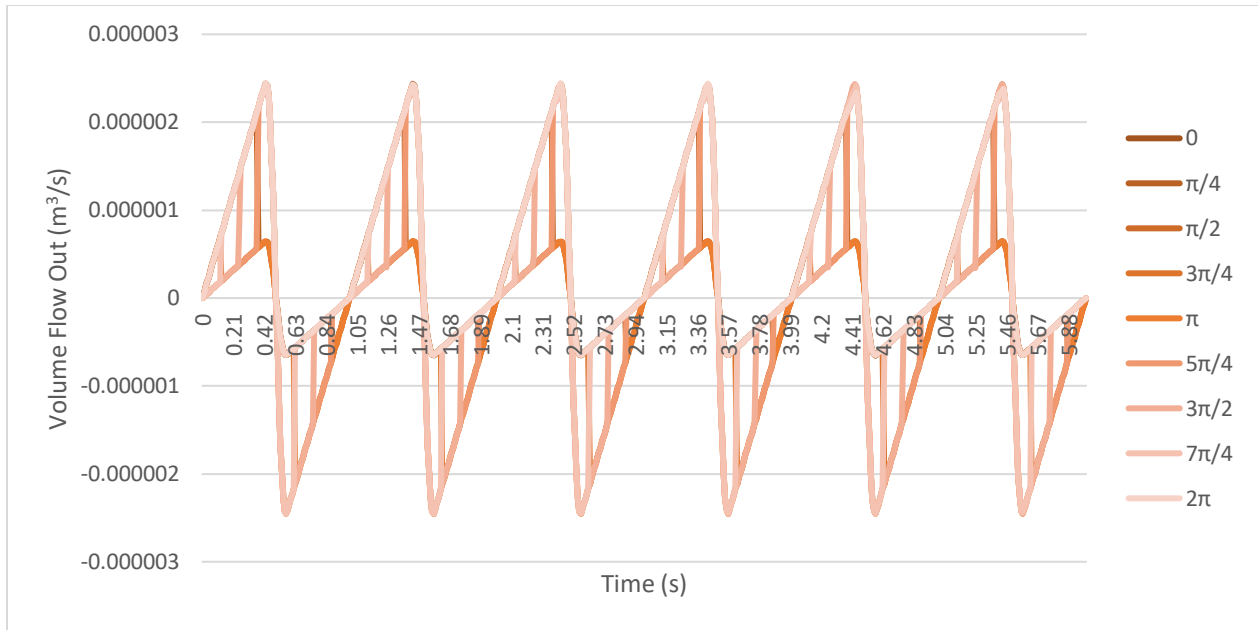


Figure 20: Volume flow rate at different valve phase offsets. Here we used a duty cycle of 50%. A net unidirectional flow can only be created when the valve phase is offset from the pump by certain amounts; some phases produce unidirectional flow in the opposite direction.

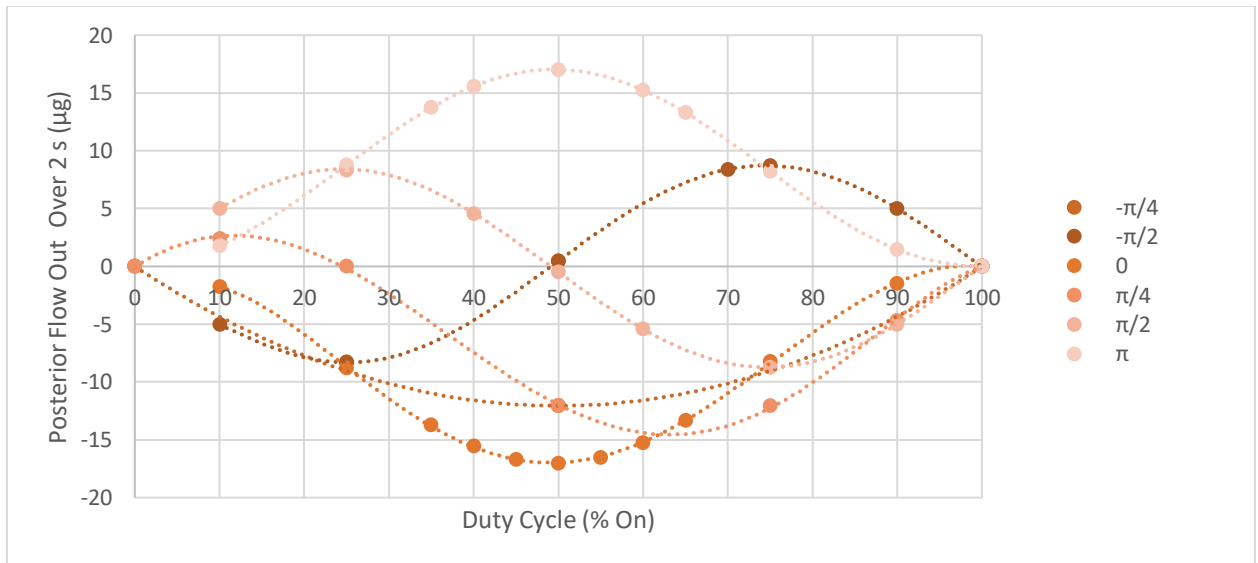


Figure 21: The effect of valve phase and duty cycle on net unidirectional flow. The optimal duty cycle for a perfect sinusoidal pump to produce unidirectional flow is 50% at a valve phase offset of π radians. Anterior flow is maximized at a valve phase offset of 0 radians.

Even actuating the system at different points (in the central chamber and in the posterior chamber) out of phase from one another, in the absence of spiracular valving, no unidirectional flow can be created. Only by incorporating spiracular valving can a net unidirectional flow be produced.

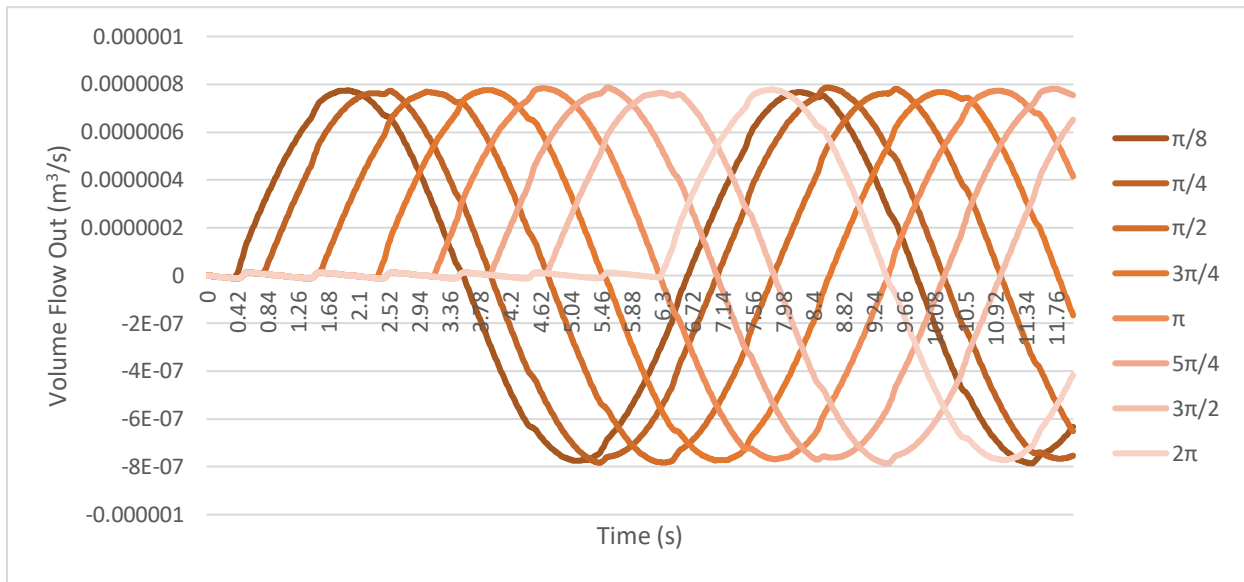


Figure 22: Delayed phase actuation without valves. The legend entries represent the phase by which the posterior actuation was delayed from the central actuation. Without valves, unidirectional flow cannot be created even with two separate pump cycles. Instead, we only see bidirectional flow at all actuation phases.

Advective flow dominated in the dorsolateral trunks and first generation of tubes, especially at low length-width ratios. There was almost no advective flow in the third generation of channels. Diffusive flow dominated in the second and third generations of tubes. As the ratio of length to width increased from 10 to 75 and up, the influence of the abdominal pump decreased, until diffusive flow completely dominated at a ratio around 75. This can be observed in the Figure 23.

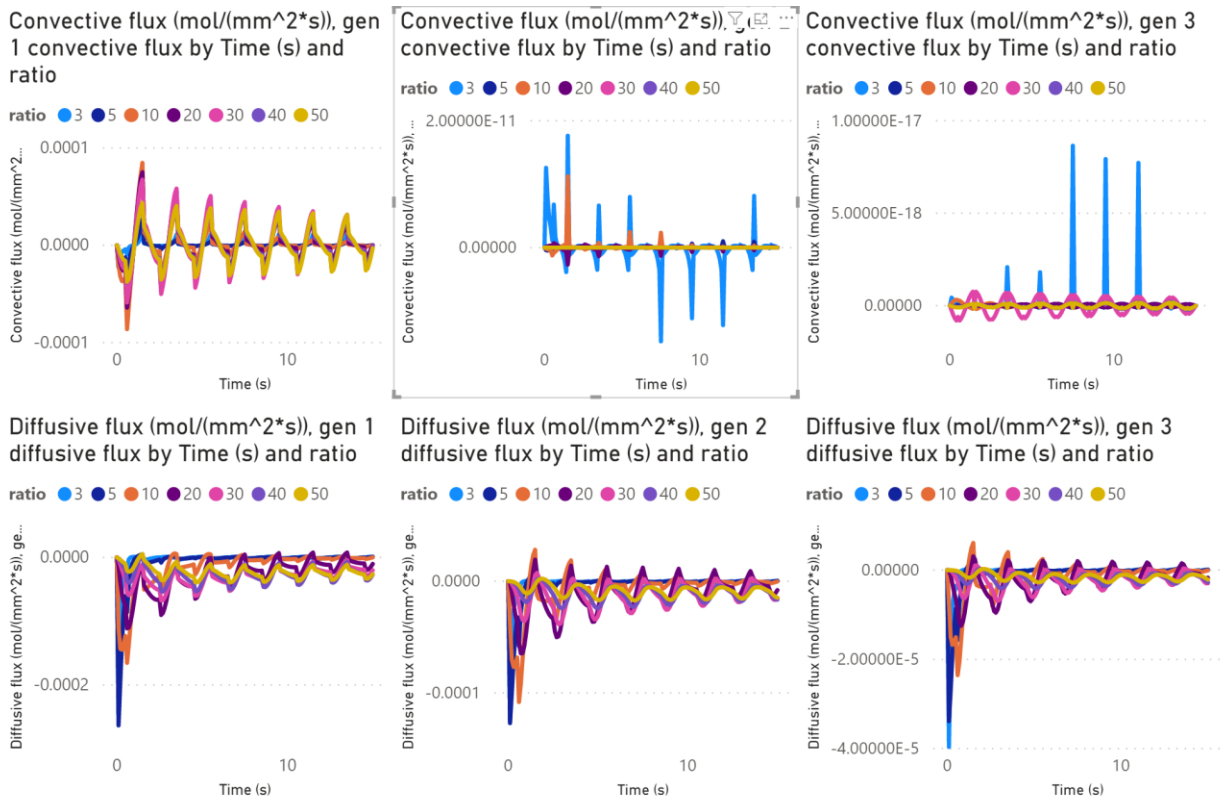


Figure 23: Advective and diffusive flux at different length-width ratios. Here we see that in the first generation, advective flux dominates, but in tube generations 2 and 3 diffusive flux dominates. The pump pattern is clearly visible at all generations but by generation 3 the advective flux is effectively zero. Diffusive flux displays strange, unintuitive patterns as the ratio changes from 3 to 50, which will be addressed in the Discussion section.

Discussion

Here we were able to study how different aspects of the insect respiratory system affect the creation of advective and diffusive flow within the tracheal network. Our parametric study allowed us to systematically examine various aspects of the insect respiratory system that cannot be easily studied *in vivo*, including valve timing and network geometry. We were able to assess the relative importance of respiratory system features in both passive and active ventilation and found that valve timing is the most important factor for the creation of net unidirectional flow, and tracheal tube length is the most important factor for determining the characteristics of diffusive flux

Abdominal pumping is a widespread behavior in insects and is often thought of as a respiratory behavior, though there may also be a circulatory role (Pendar et al., 2019). Based on the idea that tracheal tube compression is driven by the abdominal pump, the mechanics identified in this study match with what has been observed in some species of insects (Heinrich et al., 2013; Pendar et al., 2015; Waters et al., 2013). The tubes compress when the spiracular valves are open, leading to the creation of a net unidirectional flow from the anterior segment out through the posterior segments, assuming the valve and the pump are offset by the appropriate phase.

The results of this study emphasize the importance of spiracular valving in active ventilation. Offset valve phasing is essential for the creation of net unidirectional flow. In a system with no valves, no unidirectional flow can be created (see Figure 19). In a system with valves, some valve phase offsets create flow in the anterior direction, while others create flow in the posterior direction (see Figure 21). The maximum unidirectional flow in the posterior direction is created when valving is offset from pumping by π radians. The valves must be offset from the pump cycle such that flow can be drawn in and pushed out.

Given the assumptions used to create the first model – branching tracheal tubes with decreasing diameter, valves in phase with the pumps, no diffusion - we find that hydraulic resistance alone cannot create unidirectional flow (see Figure 19). Creating a gradient of hydraulic resistance, for instance by creating narrower tubes at the anterior and wider tubes at the posterior, cannot result in the creation of a net unidirectional flow in a laminar system.

There is an optimal valve duty cycle for generating unidirectional flow. For sinusoidal pumping, this duty cycle is 50% on, 50% off. At a duty cycle of 0% or 100% (always off or always on), no unidirectional flow can be created (see Figure 21). Other duty cycles can result in unidirectional flow, but the rate is reduced compared to the optimal duty cycles.

While the first part of this study was focused entirely on advective flow, and the mechanisms by which network geometry, pump phasing, and valving create a net unidirectional flow, the second part of this study advanced the model by adding a diffusive flux component. This second model enabled us to test hypotheses about the relative importance of diffusion and advection.

When diffusion is incorporated into the model, the length-to-width ratio of tracheal tubes is the most important factor for determining whether diffusive or advective flow dominates. As the relative length of the tracheal tubes increases, the influence of diffusion on flow rate increases and the effect of pumping on diffusive flux is washed out (see Figure 24). Most of the advective flow occurs in the larger tracheal tubes and longitudinal trunks, with diffusive flux being more prominent in the smaller tracheal tubes and almost no advective flux taking place. This is a necessary consequence of a system like the insect tracheal network, with blind-ended channels at the tracheole tips. Flow through the large tracheal trunks enables efficient exchange with the outside air, and diffusion within the smaller tracheal tubes allows for exchange of oxygen and carbon dioxide at the tissue sites.

Unfortunately, the results of our study on diffusive flux seem to defy physics, with flow going in the opposite direction to what might be intuited. We were unable to find a combination of simulation parameters under which flow moved from the spiracles to the tracheole tips. Whether this was a result of improperly designed simulations or an artifact of the simulation is unknown.

Future studies should attempt to clarify the differences between the properties of air and water as they apply to advective and diffusive flux. Here we assume that because the Reynolds number was matched and similar diffusion coefficients were used, we can draw conclusions about the movement of air within a similar network, but that is not necessarily justified. Future work should attempt to actually use air as the fluid studied, or fix a dimensionless parameter to match advective and diffusive fluxes.

This study can be used to inform the experimental design of future studies in living insects. Although respiratory system features cannot be varied parametrically in a single live specimen, natural variation within a species can act as a substitute for a narrow range of parameters. Future studies using simulated tracheal networks should incorporate more than three generations of tracheal tubes and expand the range of parameter values used to construct the system. Adding fluid-structure interactions could also better simulate tracheal tube compression and allow us to examine how pressure changes can actuate different types of tracheal tube compression.

This study improves our understanding of airflow within the insect respiratory system. It suggests how unidirectional flow is created within the larger tracheal trunks as well as how diffusive flux occurs throughout the system as a whole. If future studies are better able to match the actual physical parameters of the insect system, simulations can be used to make determinations about actual airflow patterns within the live insect and inform the development of studies on live insects.

Conclusion

The major goal of this dissertation was to synthesize a physiological study of insect respiratory behaviors with fluid dynamics simulations to better understand how flow is created in the insect respiratory system. To accomplish this goal, we used phase contrast x-ray, video digitization, manual tracking, and parametric fluid dynamics simulations. Specifically, within this dissertation I characterized the respiratory behaviors of the Madagascar hissing cockroach, probed the live insect system by exposing it to hypoxia and hyperoxia, and then built a model of a simplified insect respiratory system in COMSOL Multiphysics to test hypotheses about network geometry and valving.

Hissing cockroach respiratory coordination

In the first part of our study, we were interested in identifying the specific coordination of abdominal pumping, tracheal tube compression, and spiracular valving in an actively ventilating Madagascar hissing cockroach. Using phase-contrast x-ray imaging, we were able to identify patterns of tracheal compression and spiracular valving at a sub-second temporal scale with micron-level resolution. Frame-by-frame analysis of x-ray footage allowed us to assess how the animal coordinates its respiratory behaviors. We identified a consistent pattern of spiracular opening, closing, and fluttering coordinated with abdominal pumping. We also identified a consistent correlation between abdominal pumping and tracheal tube compression, suggesting that some interaction between the interstitial tissue and tracheal tubes results in their collapse when pressure is applied.

By studying the insect respiratory system in its natural state, we were able to classify the mechanical components involved in respiration, and measure how they are coordinated during active respiratory behavior. We identified consistent patterns of coordination that are most likely being used to balance unidirectional advective flow with diffusive flux to optimize gas exchange at the tissues.

The response to hypoxia and hyperoxia

Following the first study, we examined how respiratory patterns change when an insect is exposed to hyperoxic and hypoxic conditions. We found that the insect changes the frequency of its abdominal pump – and thus its tracheal compression – to alter the characteristics of gas exchange patterns in response to changing environmental conditions. The insects increase their pump frequency at lower oxygen concentrations and decrease their pump frequency at higher oxygen concentrations, most likely in order to increase advective flow when oxygen availability is limited. We also identified a change in spiracular valving behavior that may be used to further enhance diffusive gas exchange at the interface in between pumps, increasing the amount of time their spiracles remain open at lower oxygen concentrations and decreasing the amount of time their spiracles are open at higher oxygen concentration. Changes in spiracular valving may also be responsible for balancing water loss and oxidative damage as oxygen availability varies.

These results apply to one species, the Madagascar hissing cockroach, but may also apply to the respiratory behaviors of other large, active insects that may have similar respiratory requirements and behaviors. Certainly, future studies using these techniques should examine other insect species to form

a more holistic understanding of insect respiration in general. It would also be prudent to incorporate flow-through respirometry and pressure sensing into future studies to better understand gas flow patterns and the role of abdominal pumping in tracheal tube compression. These tools could advance our understanding of how airflow actually occurs in the respiratory system, as well as confirm our hypotheses about the relationship between abdominal pumping and tracheal tube compression.

Simulating the insect respiratory system

Finally, we studied the insect respiratory system in a generalized fluid dynamics simulation, albeit one based on our findings in the hissing cockroach. By constructing a parameterized insect respiratory system, we were able to study aspects of flow creation that cannot be easily studied *in vivo*. We examined the impact of network geometry and valving on the creation of both advective and diffusive flows and found that the action of the spiracular valve is of utmost importance for the creation of unidirectional flow; unidirectional advective flow cannot be created without proper valve timing. We found that network geometry alone cannot create unidirectional flow, but changes in the relative lengths of tracheal tubes have a large impact on the relative prominence of advective versus diffusive flux, especially in the smaller tracheal tubes. Higher relative lengths of tracheal tubes result in greater dominance of diffusive flux. This begins to explain how tracheal network geometry develops to optimize advective airflow in the larger tracheal tubes and diffusive flux in the smaller tracheal tubes for gas exchange at the tissues.

Future simulation studies should incorporate more complex channel geometry, such as multi-branch channels, three-dimensional channels, and channels at varying angles to better mimic the insect respiratory system. Future studies should also test the network with different fluids and pressure conditions. These will produce results that are more applicable to the natural system, and thus can be used to better inform studies in living insects.

Future work

The insect respiratory system displays many desirable aspects that could potentially be represented in an advanced microfluidic device. These include low power use, a small device size footprint, high durability, a balance between diffusive and advective fluid movement (Aboelkassem & Staples, 2013; Harrison et al., 2013) and unidirectional flow conditions (Harrison et al., 2013; Heinrich et al., 2013). It is our hope throughout this work to identify the physiological components that give rise to these properties and eventually to use that knowledge to design biologically inspired microfluidic tools. The insect respiratory system represents a low energy, single-actuation pumping network that could see application in biomedical devices such as point-of-care diagnostic screening, cancer detection, tissue engineering, and implantable microdevices.

References

- Aboelkassem, Y., & Staples, A. E. (2013). Selective pumping in a network: Insect-style microscale flow transport. *Bioinspiration and Biomimetics*, *8*(2). <https://doi.org/10.1088/1748-3182/8/2/026004>
- Ambler, G., Omar, R. Z., Royston, P., Kinsman, R., Keogh, B. E., & Taylor, K. M. (2005). Generic, simple risk stratification model for heart valve surgery. *Circulation*, *112*(2), 224–231. <https://doi.org/10.1161/CIRCULATIONAHA.104.515049>
- Askanazi, J., Milic-Emili, J., & Broell, J. R. (1979). Influence of exercise and CO₂ on breathing pattern of normal man. *Journal of Applied Physiology Respiratory Environmental and Exercise Physiology*, *47*(1), 192–196. <https://doi.org/10.1152/jappl.1979.47.1.192>
- Caretti, D. M., Szlyk, P. C., & Sils, I. V. (1992). *and respiratory timing I*, *. 90*, 201–211.
- Contreras, H. L., & Bradley, T. J. (2010). Transitions in insect respiratory patterns are controlled by changes in metabolic rate. *Journal of Insect Physiology*, *56*(5), 522–528. <https://doi.org/10.1016/j.jinsphys.2009.05.018>
- Contreras, Heidi L., Heinrich, E. C., & Bradley, T. J. (2014). Hypotheses regarding the discontinuous gas exchange cycle (DGC) of insects. *Current Opinion in Insect Science*, *4*(1), 48–53. <https://doi.org/10.1016/j.cois.2014.08.008>
- Daley, M. A., Bramble, D. M., & Carrier, D. R. (2013). Impact Loading and Locomotor-Respiratory Coordination Significantly Influence Breathing Dynamics in Running Humans. *PLoS ONE*, *8*(8). <https://doi.org/10.1371/journal.pone.0070752>
- Gelson, E., Gatzoulis, M., & Johnson, M. (2007). Pregnancy plus: Valvular heart disease. *British Medical Journal*, *335*(7628), 1042–1045. <https://doi.org/10.1136/bmj.39365.655833.AE>
- Greenlee, K. J., Montooth, K. L., & Helm, B. R. (2014). Predicting performance and plasticity in the development of respiratory structures and metabolic systems. *Integrative and Comparative Biology*, *54*(2), 307–322. <https://doi.org/10.1093/icb/icu018>
- Groenewald, B., Hetz, S. K., Chown, S. L., & Terblanche, J. S. (2012). Respiratory dynamics of discontinuous gas exchange in the tracheal system of the desert locust, *Schistocerca gregaria*. *Journal of Experimental Biology*, *215*(13), 2301–2307. <https://doi.org/10.1242/jeb.070995>
- Harak, M., Lamprecht, I., & Kuusik, A. (1996). Metabolic cost of ventilating movements in pupae of *Tenebrio molitor* and *Galleria mellonella* studied by direct calorimetry. *Thermochimica Acta*, *276*(1–2), 41–47. [https://doi.org/10.1016/0040-6031\(95\)02750-5](https://doi.org/10.1016/0040-6031(95)02750-5)
- Harrison, J. F. (2009). Tracheal System. *Encyclopedia of Insects*, 1011–1015. <https://doi.org/10.1016/B978-0-12-374144-8.00265-4>
- Harrison, J. F., Waters, J. S., Cease, A. J., Vanden Brooks, J. M., Callier, V., Jaco Klok, C., Shaffer, K., & Socha, J. J. (2013). How locusts breathe. *Physiology*, *28*(1), 18–27. <https://doi.org/10.1152/physiol.00043.2012>
- Hedrick, T. L. (2008). Software techniques for two- and three-dimensional kinematic measurements of biological and biomimetic systems. *Bioinspiration and Biomimetics*, *3*(3). <https://doi.org/10.1088/1748-3182/3/3/034001>
- Heinrich, E. C., McHenry, M. J., & Bradley, T. J. (2013). Coordinated ventilation and spiracle activity

- produce unidirectional airflow in the hissing cockroach, *Gromphadorhina portentosa*. *Journal of Experimental Biology*, 216(23), 4473–4482. <https://doi.org/10.1242/jeb.088450>
- Hetz, S. K., & Bradley, T. J. (2005). Insects breathe discontinuously to avoid oxygen toxicity. *Nature*, 433(7025), 516–519. <https://doi.org/10.1038/nature03106>
- Heymann, N., & Lehmann, F. O. (2006). The significance of spiracle conductance and spatial arrangement for flight muscle function and aerodynamic performance in flying *Drosophila*. *Journal of Experimental Biology*, 209(9), 1662–1677. <https://doi.org/10.1242/jeb.02203>
- Hillman, D. R., Murphy, A. S., Antic, R., & Pezzullo, L. (2006). The economic cost of sleep disorders. *Sleep*, 29(3), 299–305. <https://doi.org/10.1093/sleep/29.3.299>
- Hoback, W.W.; Stanley, D. W. (2001). Insects in Hypoxia. *Journal of Insect Physiology*, 47, 533–542. [https://doi.org/10.3964/j.issn.1000-0593\(2017\)06-1879-06](https://doi.org/10.3964/j.issn.1000-0593(2017)06-1879-06)
- Hudgel, D. W., Gordon, E. A., Thanakitcharu, S., & Bruce, E. N. (1998). Instability of ventilatory control in patients with obstructive sleep apnea. *American Journal of Respiratory and Critical Care Medicine*, 158(4), 1142–1149. <https://doi.org/10.1164/ajrccm.158.4.9712105>
- Kinnamon, S. C., Kammer, A. E., & Kiorpes, A. L. (1984). Control of ventilatory movements in the aquatic insect *Corydalus cornutus*: central effect of hypoxia. *Physiological Entomology*, 9(1), 19–28. <https://doi.org/10.1111/j.1365-3032.1984.tb00677.x>
- Komai, Y. (1998). Augmented respiration in a flying insect. *Journal of Experimental Biology*, 201(16), 2359–2366.
- Lancefield, T., Methley, I., Råse, U., & Kuhn, T. (2000). The application of variable event valve timing to a modern diesel engine. *SAE Technical Papers*. <https://doi.org/10.4271/2000-01-1229>
- Lehmann, F. O. (2001). Metabolic Opening During Flight *Drosophila* Spiracle. *Science*, 294(5548), 1926–1929.
- Lighton, J. R. B. (1973). Minimum cost of transport and ventilatory patterns in three African beetles. *Source: Physiological Zoology*, 46(3), 186–207. <http://www.jstor.org/stable/30155601> http://www.jstor.org/stable/30155601?seq=1&cid=pdf-reference#references_tab_contents <http://about.jstor.org/terms>
- Lighton, J. R. B. (1988). Simultaneous measurement of oxygen uptake and carbon dioxide emission during discontinuous ventilation in the tok-tok beetle, *Psammodes striatus*. *Journal of Insect Physiology*, 34(5), 361–367. [https://doi.org/10.1016/0022-1910\(88\)90104-7](https://doi.org/10.1016/0022-1910(88)90104-7)
- Lucía, A., Carvajal, A., Calderón, F. J., Alfonso, A., & Chicharro, J. L. (1999). Breathing pattern in highly competitive cyclists during incremental exercise. *European Journal of Applied Physiology and Occupational Physiology*, 79(6), 512–521. <https://doi.org/10.1007/s004210050546>
- Mathew, O. P., & Farber, J. P. (1983). Effect of upper airway negative pressure on respiratory timing. *Respiration Physiology*, 54(2), 259–268. [https://doi.org/10.1016/0034-5687\(83\)90062-2](https://doi.org/10.1016/0034-5687(83)90062-2)
- Nelson, M. C. (1979). Sound production in the cockroach, *Gromphadorhina portentosa*: The sound-producing apparatus. *Journal of Comparative Physiology* □ A, 132(1), 27–38. <https://doi.org/10.1007/BF00617729>
- Nouhov, D. F. (2004). Investigation of the effect of inlet valve timing on the gas exchange process in

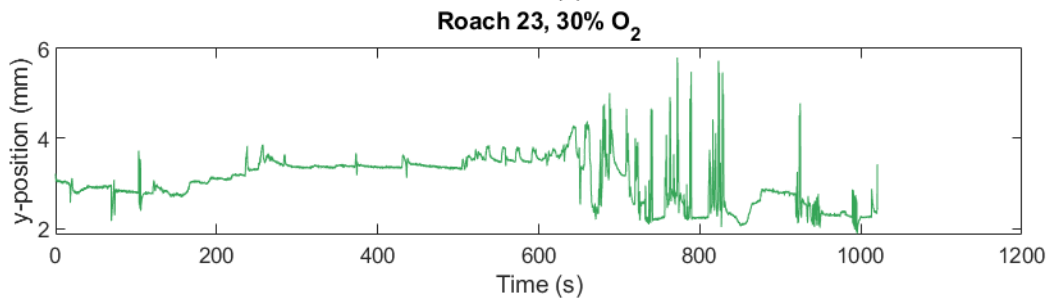
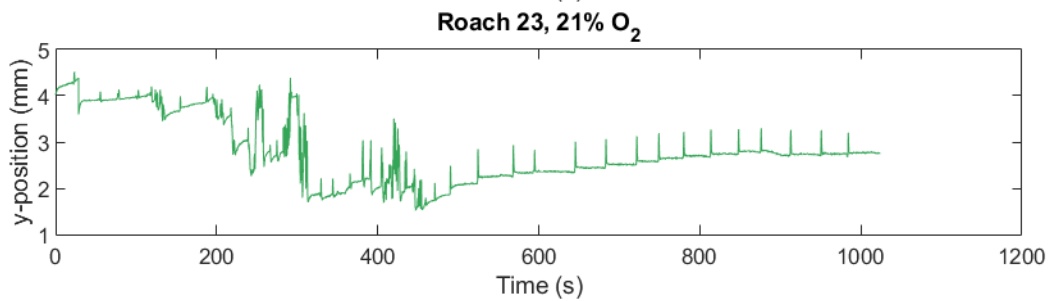
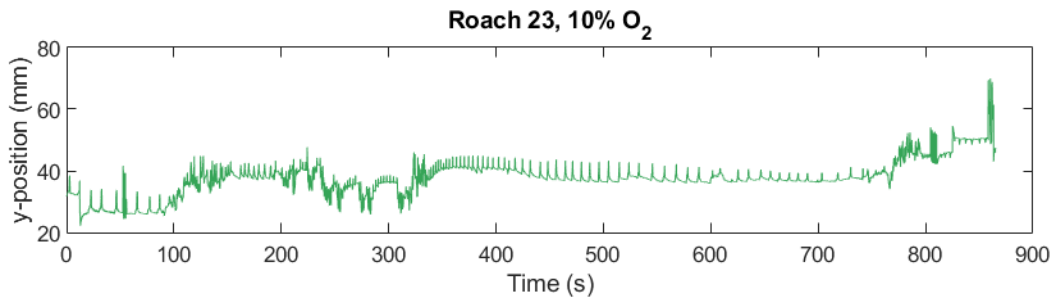
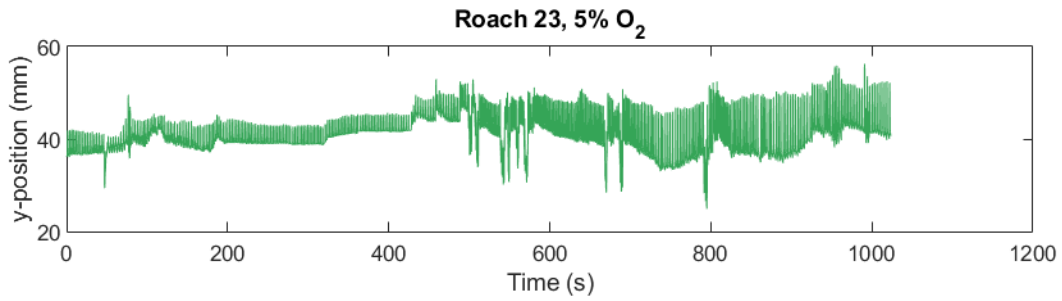
high-speed engines. *Loughborough University, Doctoral d.*

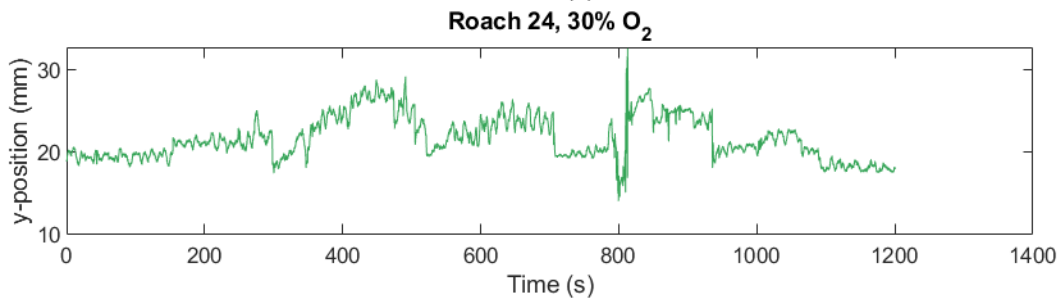
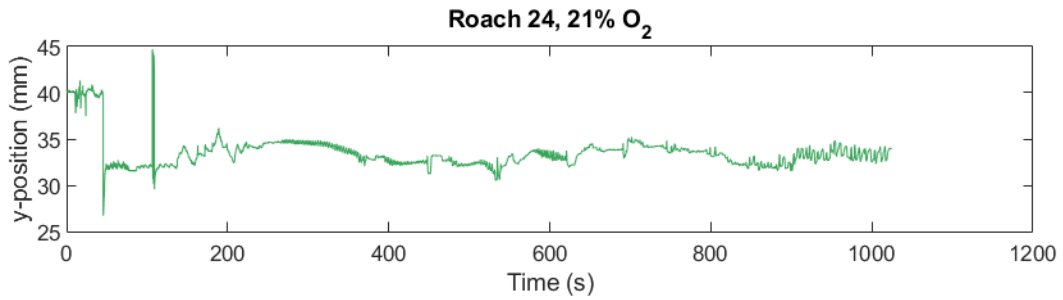
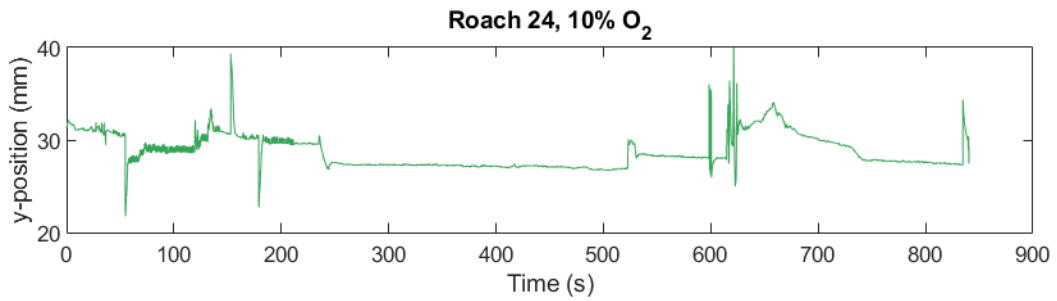
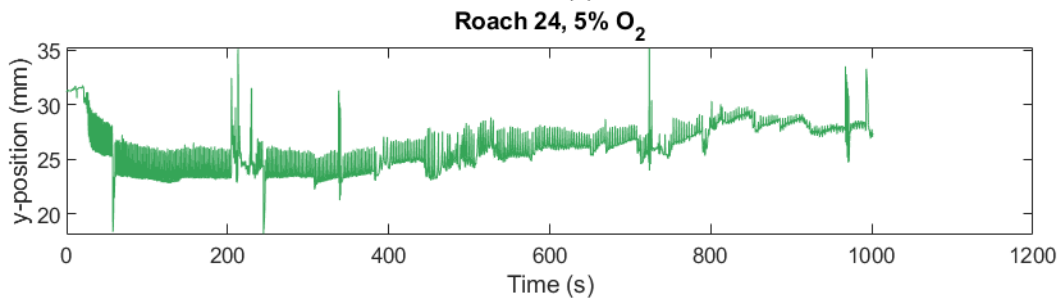
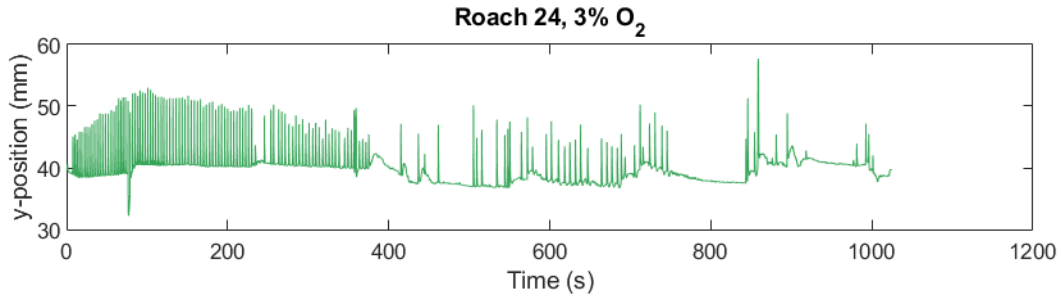
- Parker, G. A., & Smith, J. M. (1990). Optimality theory in evolutionary biology. In *Nature* (Vol. 348, Issue 6296, pp. 27–33). <https://doi.org/10.1038/348027a0>
- Pendar, H., Aviles, J., Adjerid, K., Schoenewald, C., & Socha, J. J. (2019). Functional compartmentalization in the hemocoel of insects. *Scientific Reports*, *9*(1), 1–12. <https://doi.org/10.1038/s41598-019-42504-3>
- Pendar, H., Kenny, M. C., & Socha, J. J. (2015). Tracheal compression in pupae of the beetle *Zophobas morio*. *Biology Letters*, *11*(6). <https://doi.org/10.1098/rsbl.2015.0259>
- Pendar, H., Socha, J. J., & Chung, J. (2016). Recovering signals in physiological systems with large datasets. *Biology Open*, *5*(8), 1163–1174. <https://doi.org/10.1242/bio.019133>
- Schindelin, J., Arganda-Carreras, I., Frise, E., Kaynig, V., Longair, M., Pietzsch, T., Preibisch, S., Rueden, C., Saalfeld, S., Schmid, B., Tinevez, J. Y., White, D. J., Hartenstein, V., Eliceiri, K., Tomancak, P., & Cardona, A. (2012). Fiji: An open-source platform for biological-image analysis. *Nature Methods*, *9*(7), 676–682. <https://doi.org/10.1038/nmeth.2019>
- Schmitz, A., & Harrison, J. F. (2004). Hypoxic tolerance in air-breathing invertebrates. *Respiratory Physiology and Neurobiology*, *141*(3), 229–242. <https://doi.org/10.1016/j.resp.2003.12.004>
- Schneider, C. A., Rasband, W. S., & Eliceiri, K. W. (2012). NIH Image to ImageJ: 25 years of image analysis. *Nature Methods*, *9*(7), 671–675. <https://doi.org/10.1038/nmeth.2089>
- Sherman, T. F. (1981). On connecting large vessels to small. *Journal of General Physiology*, *78*(4), 431–453. <https://doi.org/10.1085/jgp.78.4.431>
- Simelane, S. M., Abelman, S., & Duncan, F. D. (2014). Dynamics of the oxygen, carbon dioxide, and water interaction across the insect spiracle. *Abstract and Applied Analysis*, 2014. <https://doi.org/10.1155/2014/157573>
- Simelane, S. M., Abelman, S., & Duncan, F. D. (2016). Gas Exchange Models for a Flexible Insect Tracheal System. *Acta Biotheoretica*, *64*(2), 161–196. <https://doi.org/10.1007/s10441-016-9278-z>
- Socha, J. J., & De Carlo, F. (2008). Use of synchrotron tomography to image naturalistic anatomy in insects. *Developments in X-Ray Tomography VI*, 7078, 70780A. <https://doi.org/10.1117/12.795210>
- Stein, R. A., Galietti, K. M., & Leone, T. G. (2014). Dual Equal VCT A Variable Camshaft. *SAE Technical Papers*, 412.
- Tartes, U., Kuusik, A., Hiisaar, K., Metspalu, L., & Vanatoa, A. (2000). Abdominal movements, heartbeats and gas exchange in pupae of the Colorado potato beetle, *Leptinotarsa decemlineata*. *Physiological Entomology*, *25*(2), 151–158. <https://doi.org/10.1046/j.1365-3032.2000.00180.x>
- Vrtar, A., Toogood, C., Keen, B., Beeman, M., & Contreras, H. L. (2018). The effect of ambient humidity on the metabolic rate and respiratory patterns of the hissing cockroach, *Gromphadorhina portentosa* (Blattodea: Blaberidae). *Environmental Entomology*, *47*(2), 477–483. <https://doi.org/10.1093/ee/nvx208>
- Wasserthal, L. T., & Frohlich, A. S. (2017). Structure of the thoracic spiracular valves and their contribution to unidirectional gas exchange in flying blowflies *Calliphora vicina*. *Journal of Experimental Biology*, *220*(2), 208–219. <https://doi.org/10.1242/jeb.149013>

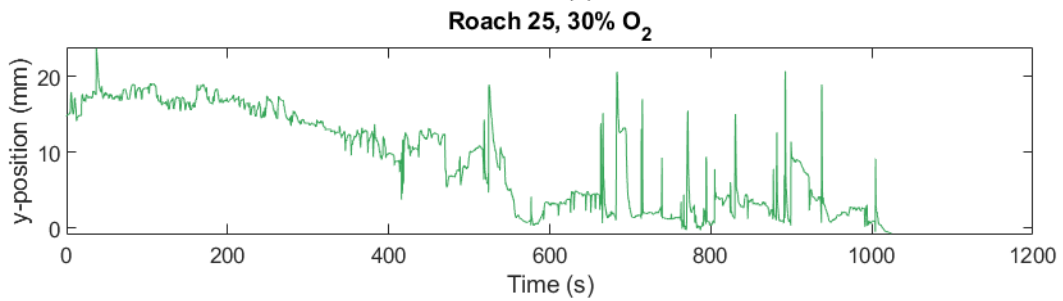
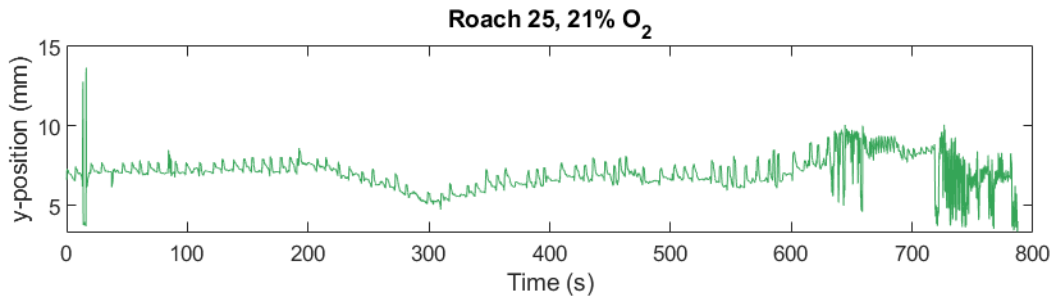
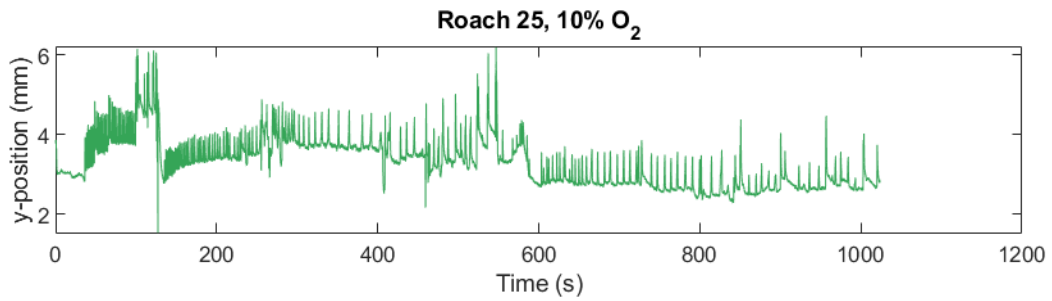
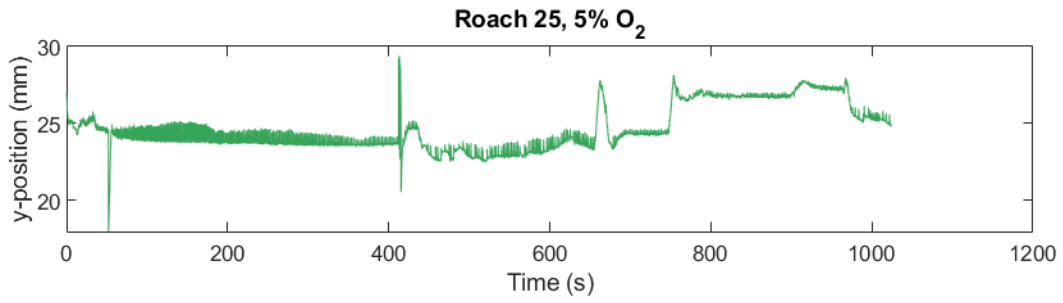
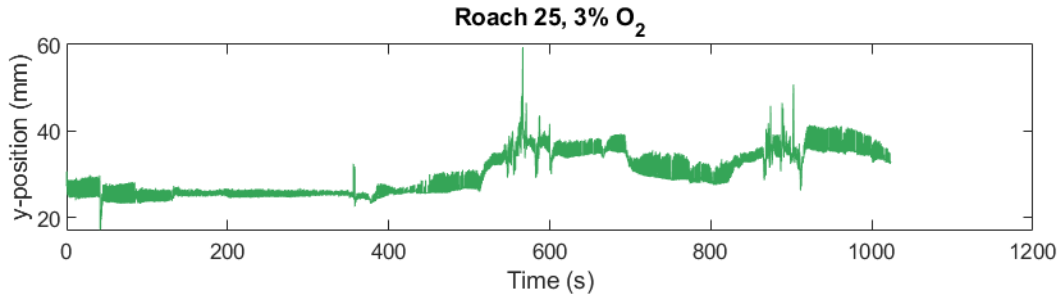
- Waters, J. S., Lee, W. K., Westneat, M. W., & Socha, J. J. (2013). Dynamics of tracheal compression in the horned passalus beetle. *American Journal of Physiology - Regulatory Integrative and Comparative Physiology*, 304(8). <https://doi.org/10.1152/ajpregu.00500.2012>
- Webster, M. R., De Vita, R., Twigg, J. N., & Socha, J. J. (2011). Mechanical properties of tracheal tubes in the American cockroach (*Periplaneta americana*). *Smart Materials and Structures*, 20(9). <https://doi.org/10.1088/0964-1726/20/9/094017>
- Wellman, A., Jordan, A. S., Malhotra, A., Fogel, R. B., Katz, E. S., Schory, K., Edwards, J. K., & White, D. P. (2004). Ventilatory control and airway anatomy in obstructive sleep apnea. *American Journal of Respiratory and Critical Care Medicine*, 170(11), 1225–1232. <https://doi.org/10.1164/rccm.200404-510OC>

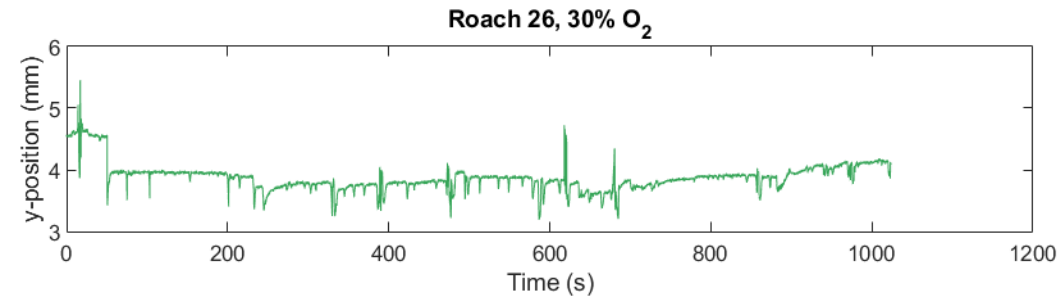
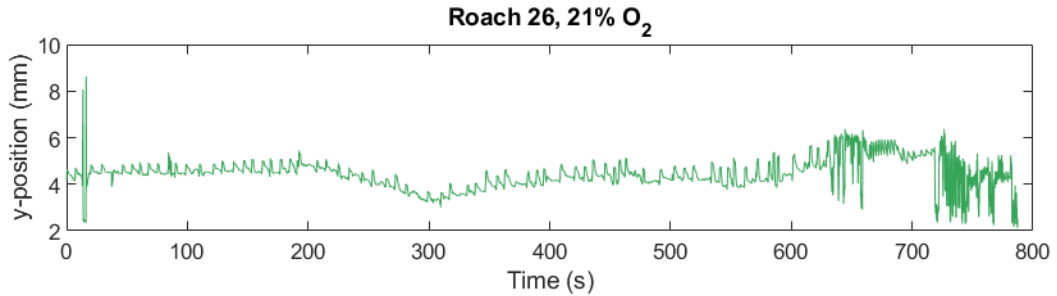
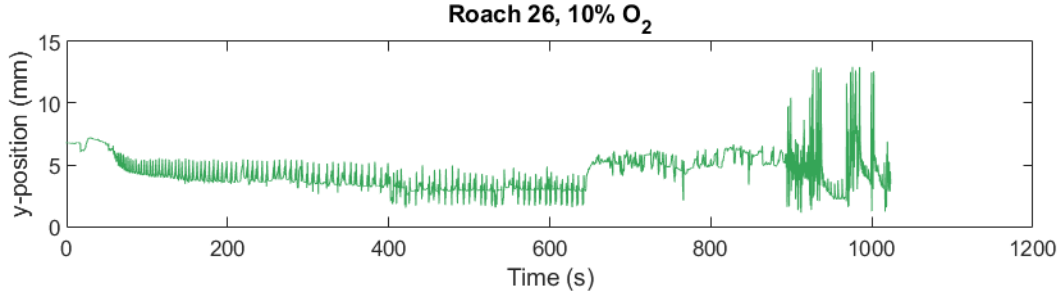
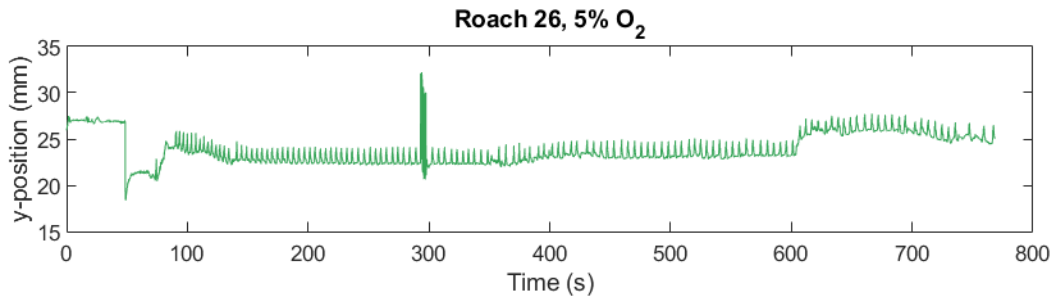
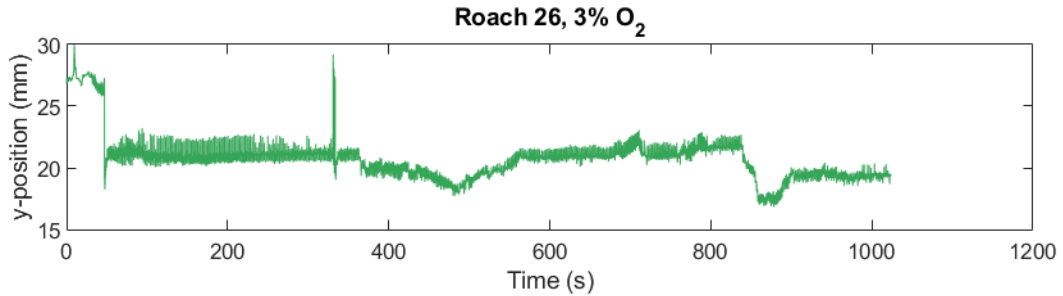
Appendix A – Plots of abdominal movement

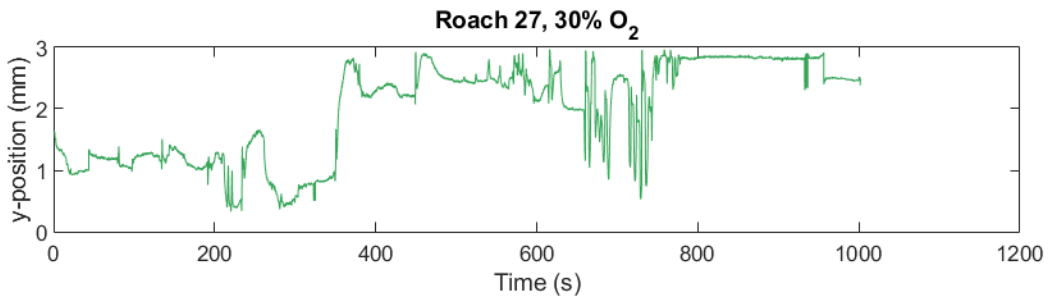
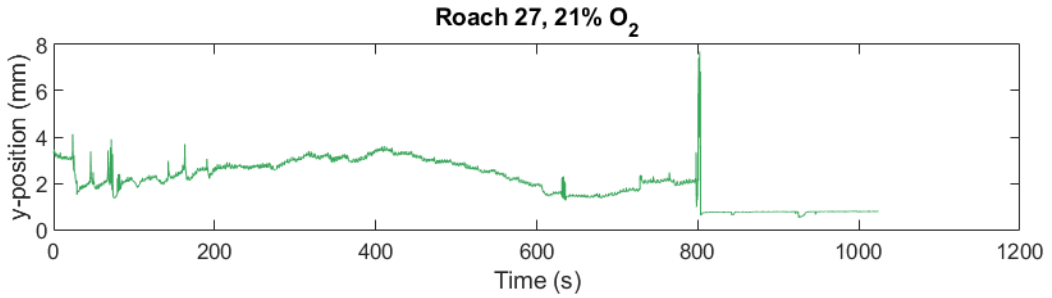
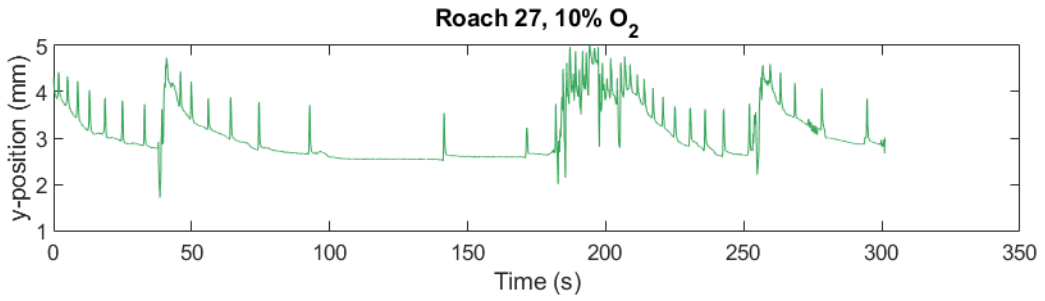
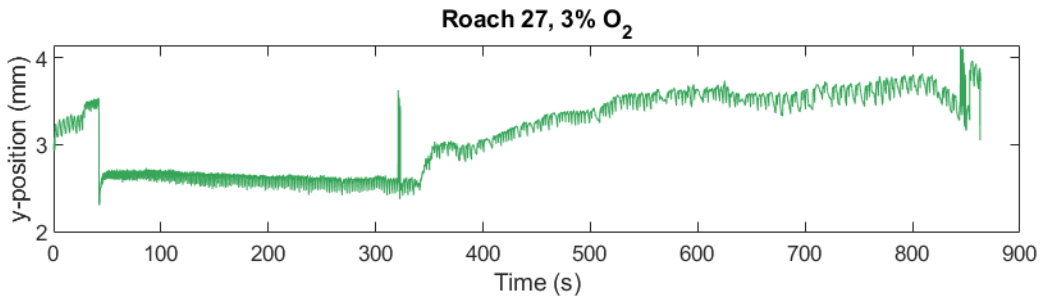
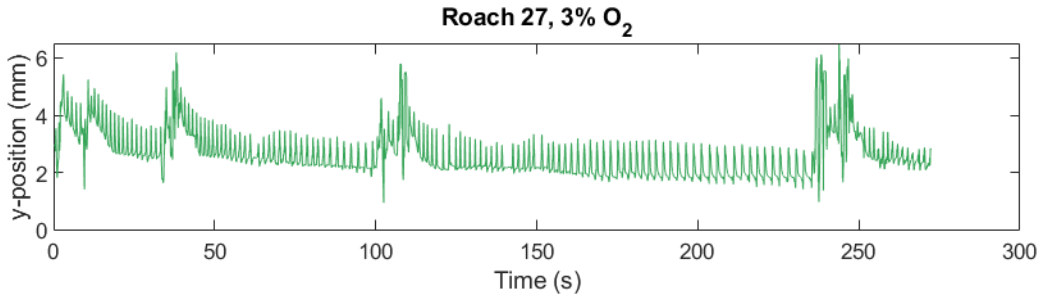
Plots of abdominal movement at different O₂ concentrations. Peaks represent abdominal pumps.

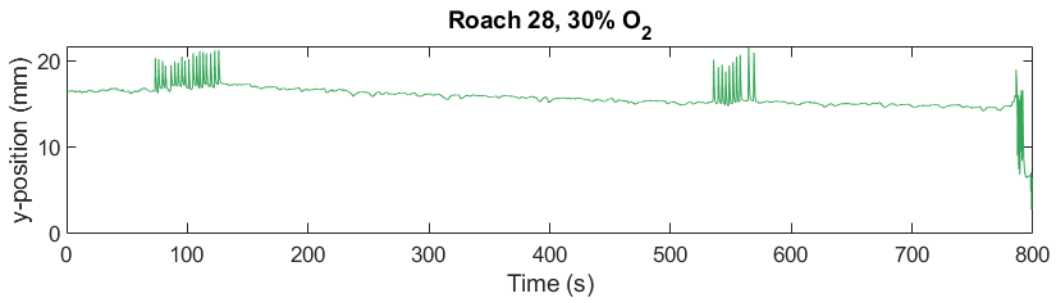
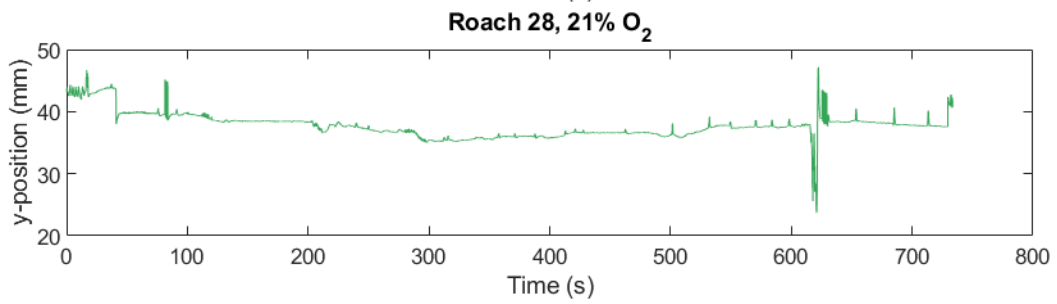
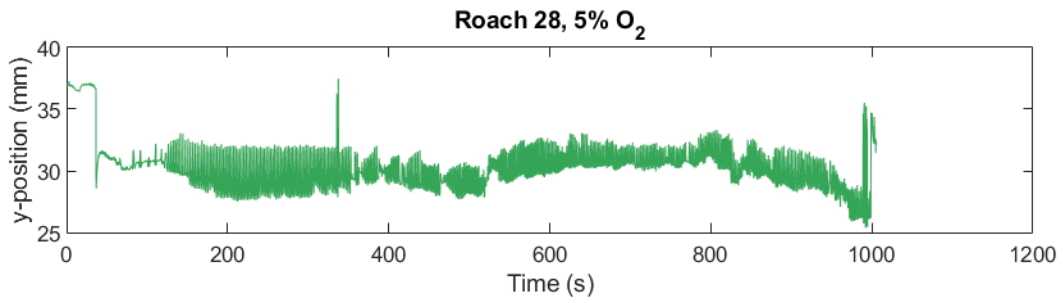
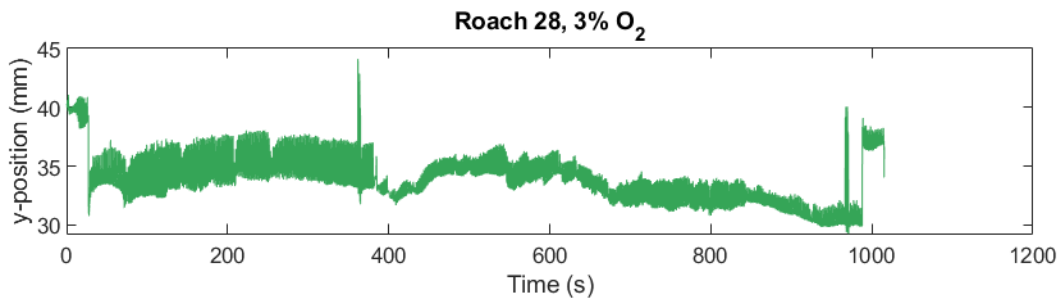






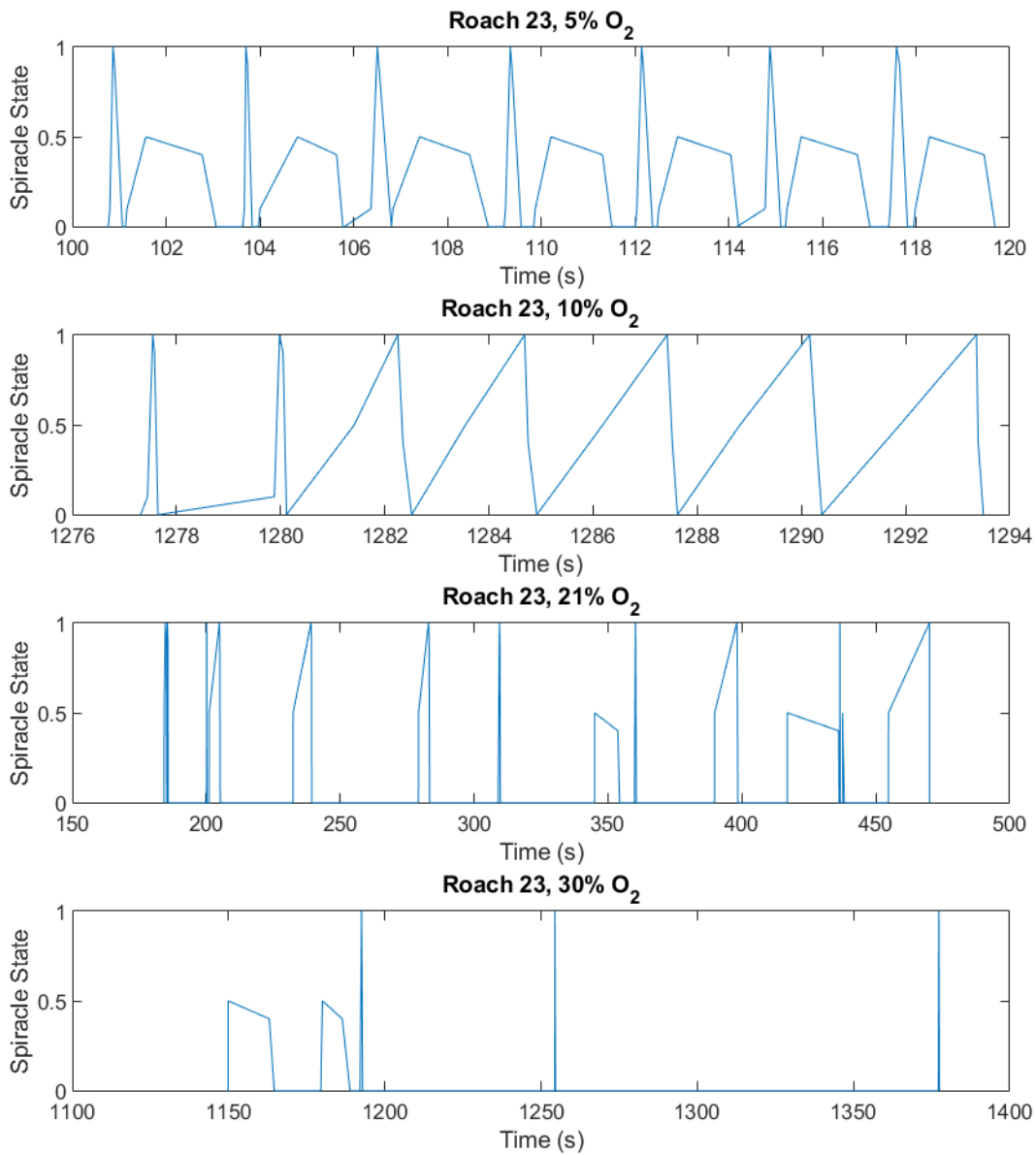


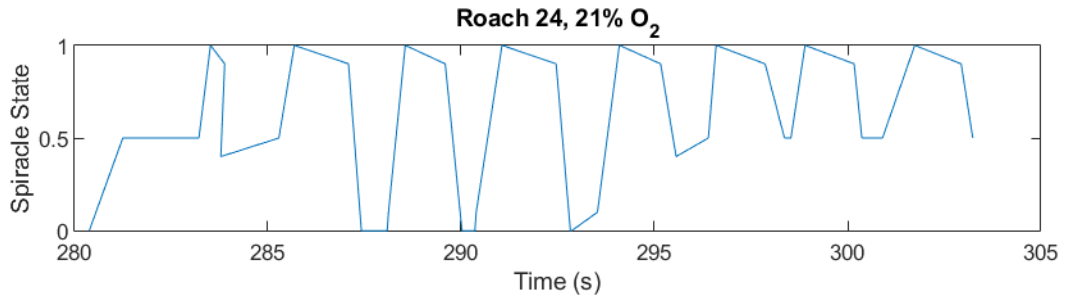
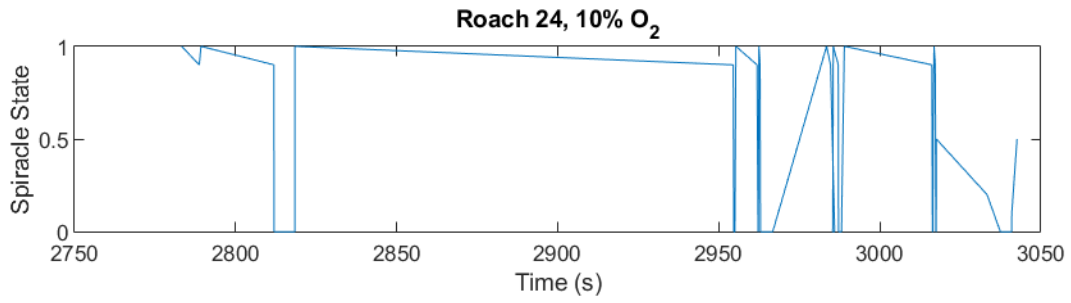
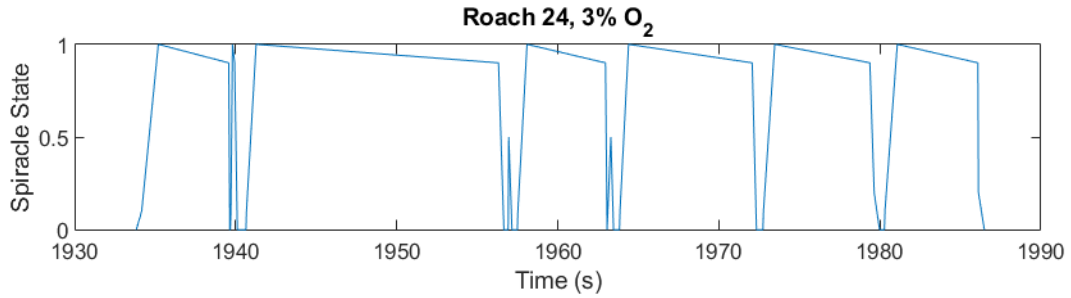


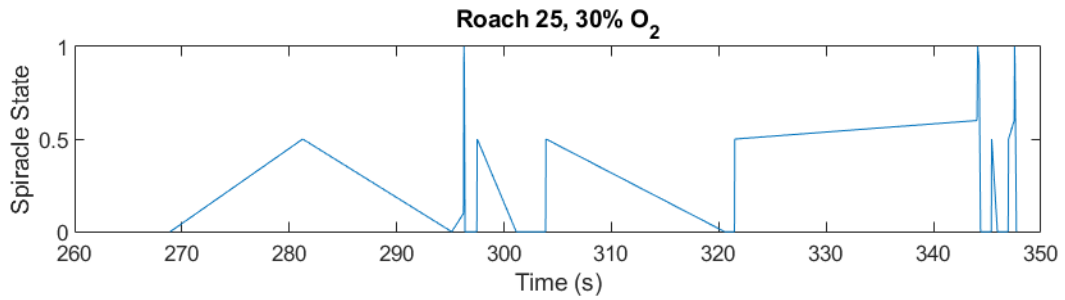
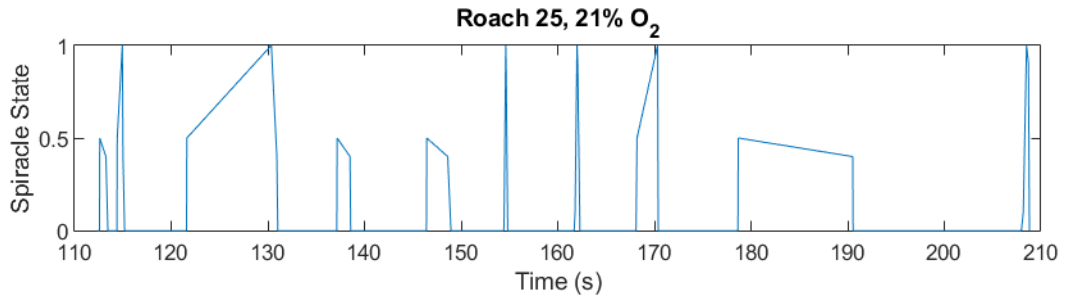
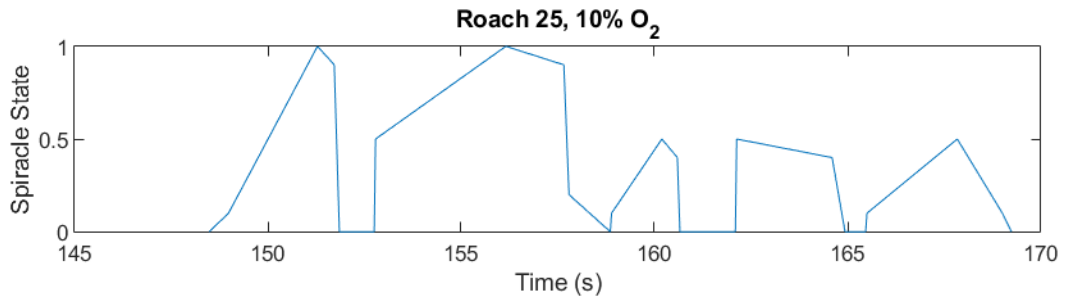
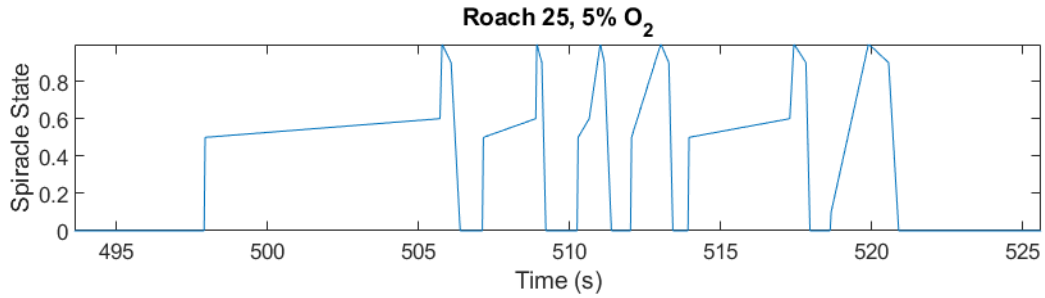


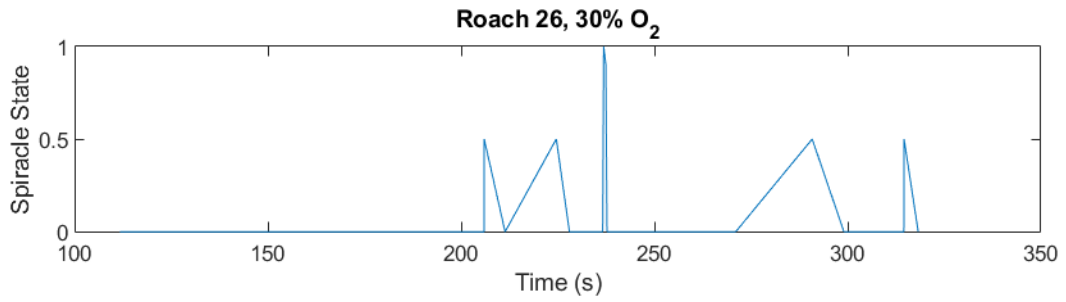
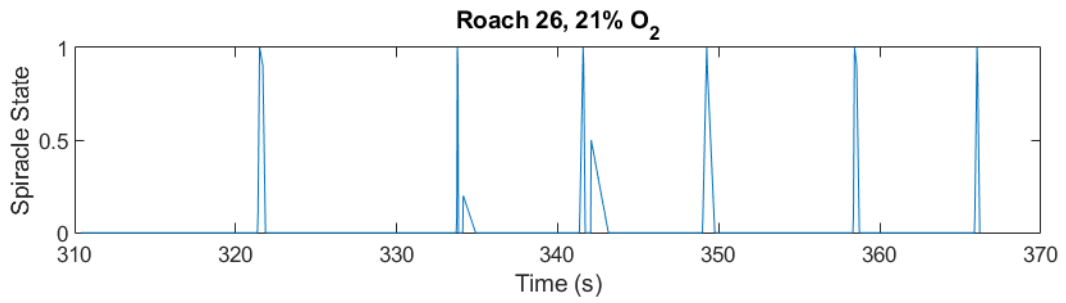
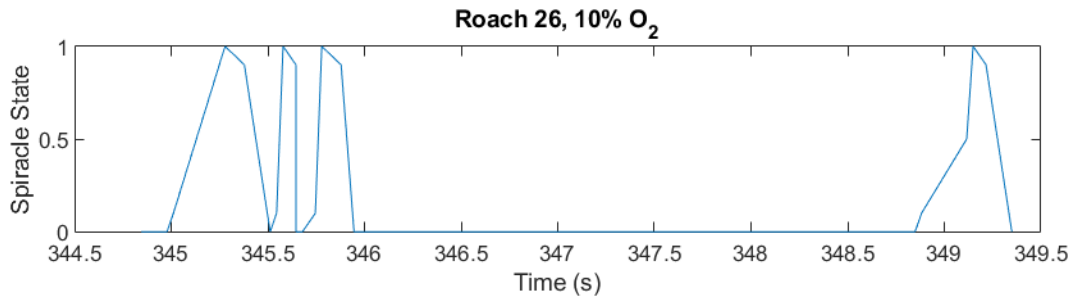
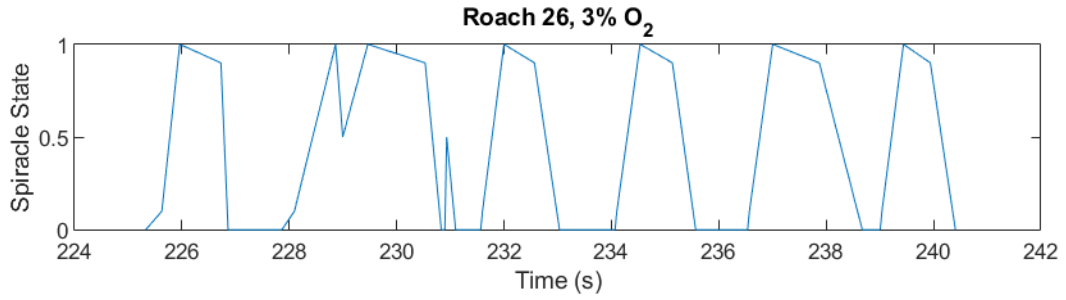
Appendix B – Plots of spiracle state

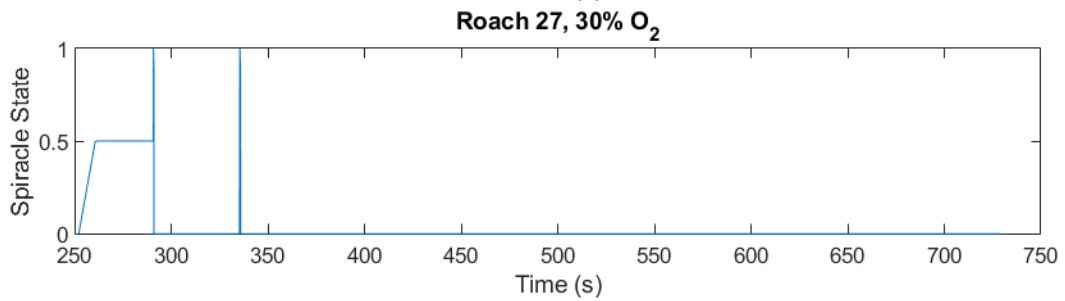
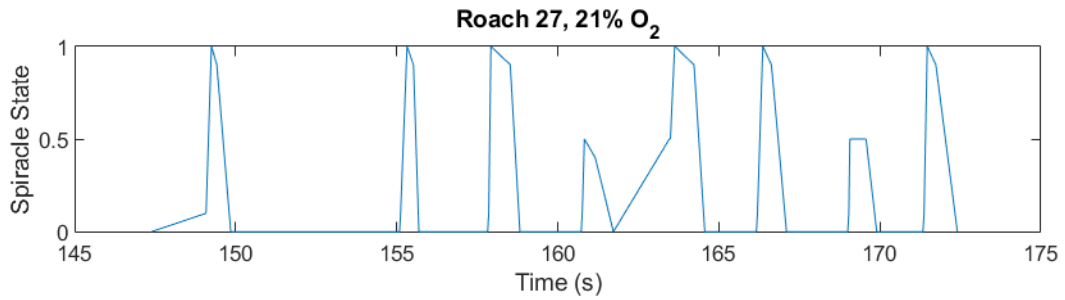
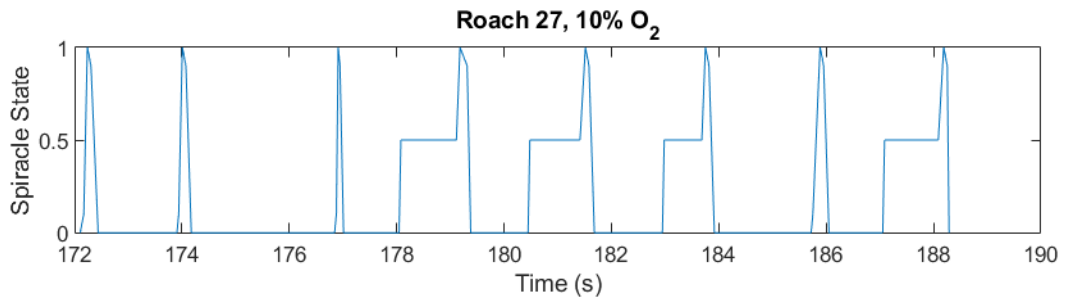
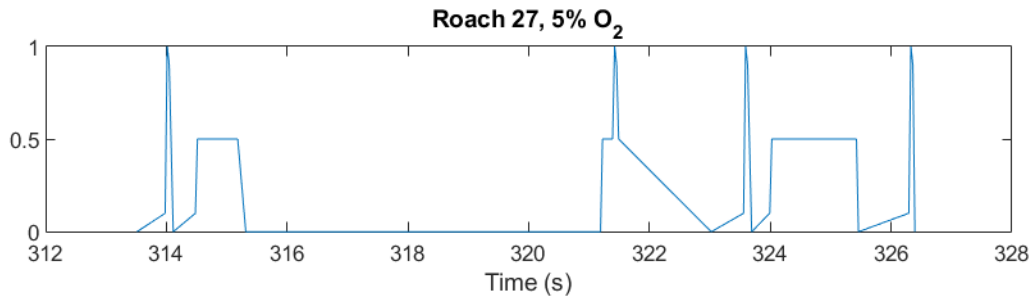
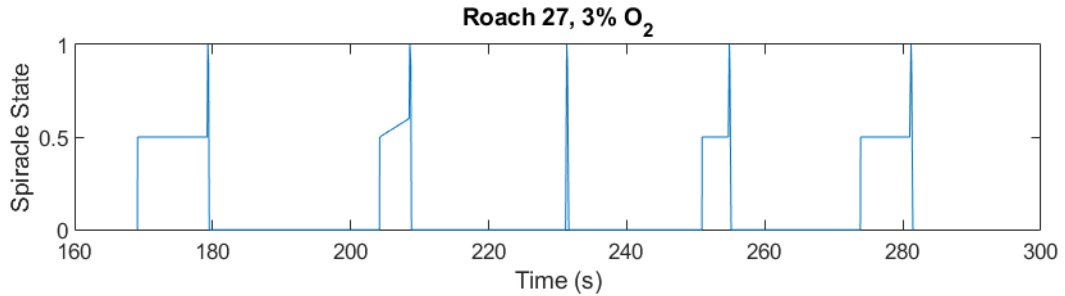
Plots of spiracle state at different O₂ concentrations. A value of 0 means the spiracle is fully closed and a value of 1 means the spiracle is fully open. Intermediate values represent fluttering.

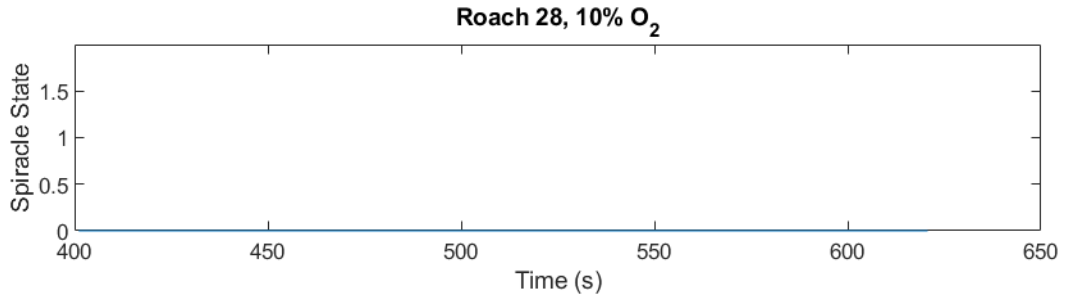
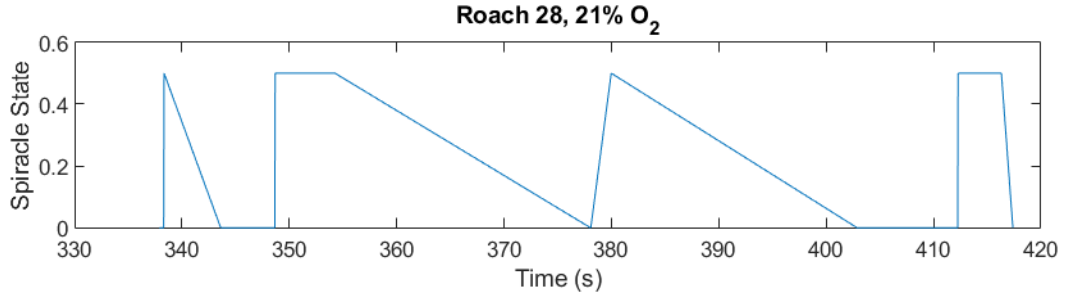
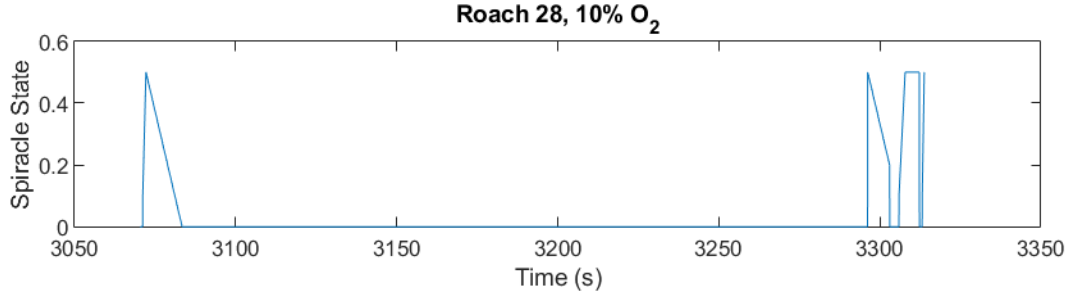
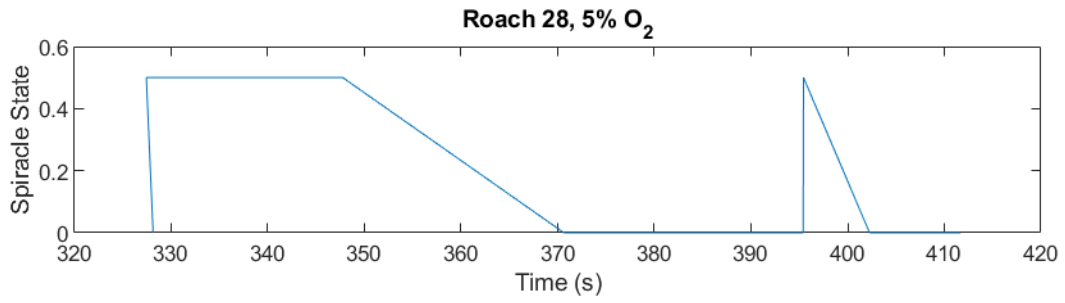
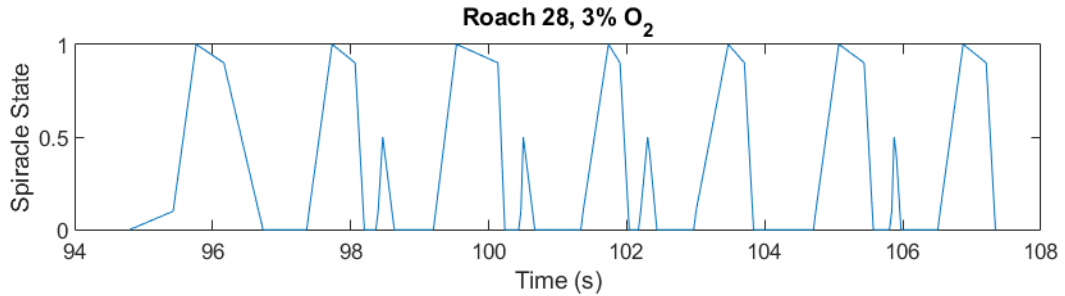

































Appendix C – COMSOL Setups

Screenshots of various states used for COMSOL simulations

- ▼  Geometry 1
 -  thorax valves (*r16*)
 -  thx first channel (*r1*)
 -  thx gen0cross (*r12*)
 -  thx gen1 (*r2*)
 -  thx gen1cross (*r13*)
 -  thx gen2 (*r4*)
 -  thx gen2cross (*r14*)
 -  thx gen3 (*r6*)
 -  trach uptake (*r21*)
 -  DL trunks (*r17*)
 -  thx mirror 1 (*mir3*)
 -  thx mirror 2 (*mir4*)
 -  thx mirror 3 (*mir5*)
 -  thx mirror 4 (*mir1*)
 -  copy thx to abd (*mov1*)
 -  Scale 1 (*sca1*)
 -  copy thx to head (*mov2*)
 -  Scale 2 (*sca2*)
 -  top lateral trunk (*r19*)
 -  bottom lateral trunk (*r20*)
 -  lateral mirror (*mir6*)
 -  Form Union (*fin*)

